HYDROCARBON POTENTIAL OF PENNSYLVANIAN BLACK SHALE RESERVOIRS, PARADOX BASIN, SOUTHEASTERN UTAH

by
S. Robert Bereskin and John McLennan

OPEN-FILE REPORT 534
UTAH GEOLOGICAL SURVEY
a division of
Utah Department of Natural Resources
2008

HYDROCARBON POTENTIAL OF PENNSYLVANIAN BLACK SHALE RESERVOIRS, PARADOX BASIN, SOUTHEASTERN UTAH

by
S. Robert Bereskin, Bereskin and Associates, Salt Lake City, Utah 84109
and
John McLennan, University of Utah, Salt Lake City, Utah 84112

Cover photo:
Shale in the Pennsylvanian Paradox Formation exposed along the Honaker Trial, San Juan County, Utah.
Photo by Craig D. Morgan.

Disclaimer

This open-file report was prepared by the authors under contract to the Utah Department of Natural Resources, Utah Geological Survey. The report has not undergone the full UGS review process, and may not necessarily conform to UGS technical, editorial, or policy standards. Therefore, it may be premature for an individual or group to take action based on its content.

The Utah Department of Natural Resources, Utah Geological Survey, makes no warranty, expressed or implied, regarding the suitability of this product for a particular use. The Utah Department of Natural Resources, Utah Geological Survey, shall not be liable under any circumstances for any direct, indirect, special, incidental, or consequential damages with respect to claims by users of this product.

OPEN-FILE REPORT 534
UTAH GEOLOGICAL SURVEY
a division of
Utah Department of Natural Resources
2008

TABLE OF CONTENTS

ABSTRACT 1
INTRODUCTION 1
GEOLOGY/GEOCHEMISTRY 1
NATURAL FRACTURES 4
GEOLOGIC/GEOCHEMICAL RESULTS 4
MECHANICAL PROPERTIES 7
    Triaxial Compression Testing 7
CONCLUSIONS AND POSSIBLE FUTURE WORK 15
    Conclusions 15
    Future Work 15
REFERENCES 19
APPENDIX A - CORE GRAPHS A-1
APPENDIX B - THIN SECTION ANALYSIS B-1
APPENDIX C - SCANNING ELECTRON MICROSCOPY C-1
APPENDIX D - FRACTURE ANALYSIS - JEFFERSON STATE 4-1 ..... D-1
APPENDIX E - XRD MULE 31-K E-1

LIST OF FIGURES

Figure 1. Gamma ray and sonic log of the Duncan Shell Government well 2
Figure 2. Kerogen type determination from TOC and Rock-Eval pyrolysis data 3
Figure 3. Variation of laboratory and logging-predicted values for Poisson's ratio 10
Figure 4. Variation of static and dynamic laboratory values for Poisson's ration 11
Figure 5. Variation of static and dynamic laboratory values for Young's modulus 11
Figure 6. Calibrated logging values for Young's modulus and the discrete laboratory measurements that were used for calibration 12
Figure 7. Laboratory measured data plotted against the sonic porosity with an annotation of linear regression fits 13
Figure 8. Logging inference of in-situ strength 14
Figure 9. Logging inference of brittleness 16
Figure 10. Expanded view of the Gothic shale - logging inference of brittleness 17
Figure 11. Vertical variation in the minimum horizontal stress 18

LIST OF TABLES

Table 1. Composite geochemical table 3
Table 2. Petrophysical laboratory measurements 6
Table 3. Summary of triaxial compression tests from the Jefferson State 4-1 core 7
Table 4. Dynamic mechanical properties determined during triaxial compression testing 8

ABSTRACT

Thin section and scanning electron microscopy evaluations, geochemical measurements and rock mechanics testing are reported for the Hovenweep, Gothic and Chimney Rock shales from two wells in the Paradox Basin, San Juan County, Utah. The evaluations indicate that these Pennsylvanian "black shale" units are likely another representation in a series of emerging resource plays. Interbedded dolomites and calcareous mudstones were also highlighted as potentially productive zones. For example, much of the fracturing mapped in this limited program occurred in the associated dolomites.

INTRODUCTION

The inspiration for this project emanated directly from a lengthy continuous core taken from the Jefferson State 4-1 well, section 4, T33S, R24E, San Juan County, Utah. Crownquest Operating and Lynden Ventures then gave permission to utilize and to study the core in hopes of clarifying the unconventional hydrocarbon potential, particularly of the Hovenweep and subjacent Gothic "shales" as recovered in that well. A fairly complete suite of logs is publicly available, as well as a particularly informative mud log. Additionally, Crownquest took some sidewall cores in the subjacent Chimney Rock shale, and these were particularly helpful for some scanning electron microscopy as appended. Furthermore, some geochemical analyses data, proprietary to Crownquest, were made available to this endeavor.

Many tasks were performed for this study, geological and geochemical procedures included the following: (1) formulation of stratigraphic coregraphs reflecting the megascopic summary on a foot-by-foot basis, (2) natural fracture summary associated with the megascopic observations, (3) geochemical data involving basic total organic carbon (TOC) measurements as well as maturation data from Rock-Eval pyrolysis and vitrinite reflectance procedures, and (4) thin section and scanning electron microscopy (SEM) photomicrographs. Important laboratory measurements include the porosity/ permeability/saturation data gleaned from the Tight Rock Analysis (TRA), as performed by TerraTek from Salt Lake City. TerraTek also took several plugs for rock mechanics purposes; most testing involved both static and acoustic analyses. This latter group of tests was intended to shed better light on in-situ stress regimes and mechanical properties – with subsequent utility for stimulation and completion design (hydraulic fracturing, log calibration, horizontal well stability, etc.).

Another set of cores from more southerly portions of the Paradox Basin were available for some use as provided by the Utah Core Research Center. One well belonging to Harken Energy was called the Mule 31-K, section 31, T41S, R24E, which successfully cored both the Gothic and underlying Chimney Rock shales. Core description was also performed on these shales, and some thin section/SEM data were also obtained. Finally, a third well drilled by Chuska Energy in 1991, the Anasazi 5L, section 5, T42S, R24E, contained a core from the Chimney Rock shale — sample core description was performed for this stratigraphic interval.

GEOLOGY/GEOCHEMISTRY

In any examination of the three pertinent shale units from youngest to oldest, Hovenweep, Gothic, and Chimney Rock (Figure 1), it is important to remember that these shales are stratigraphically separated from one another by a cyclical sequence of mostly carbonate/evaporite lithologies with subordinate amounts of terrigenous clastics, all lithologies belonging to the well-known Upper Ismay, Lower Ismay, and Desert Creek cycles in descending stratigraphic order.

In terms of the coregraphs presented

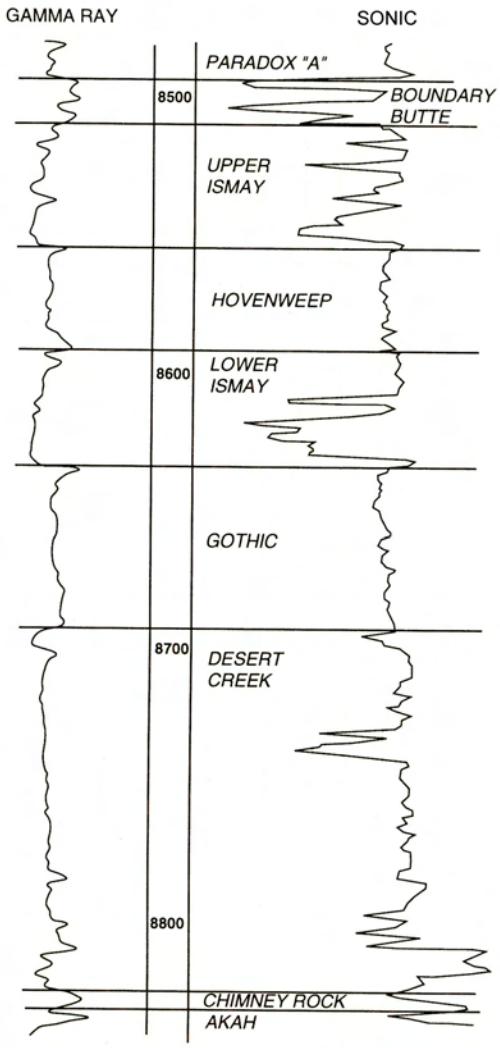

Figure 1. Gamma Ray and sonic log of the Duncan Shell Government well in section 31, T. 37 N., R. 13 W., Colorado, illustrating the stratigraphic column discussed in this report. Modified from Harr, 1996.

(Appendix A), the wells contained more core than actually presented in the coregraphs; however, the salient portions of the cores were presented in portions stratigraphically proximal to the shales themselves. The lowest unit studied, the Chimney Rock shale, was adequately represented in the Mule 31-K well and in some sidewall cores from the Jefferson State 4-1. This lowest shale unit contained various percentages of dolomite, including beds or intervals of a medium brown color which represented relatively pure dolostone material, and in fact, the Chimney Rock passed upward into dolomites of the Desert Creek cycle. The next highest mudrock, the Gothic shale, was consistently a dark brown gray calcareous mudstone for most of its stratigraphic extent. Some interbedded dolostone was subordinately present. The Gothic was naturally fractured especially in the Jefferson State core. Finally, the stratigraphically highest shale, the Hovenweep also seemed consistent if not monotonous in its calcareous mudstone content.

The basic lithology of the three shales is fairly consistent in all cases, as seen in both the megascopic and microscopic documentation. From a megascopic perspective, all shales are mostly dark brown gray, wavy to planar laminated, calcareous mudstones. The rocks are very organic looking because of the dark hues, and TOC measurements reflect a modest but significant degree of organic richness (Table 1; Figure 2). Higher TOC values would be evident if it were not for the dilution phenomenon attributable to significant percentages of terrigenous silt, various clays, pyrite, phosphate and variable quantities of diagenetic dolomite. Ostensibly, any calcite percentage would not dilute the TOC measurements due to selective removal of this carbonate mineral prior to TOC testing. Maturation measurements, Rock-Eval and vitrinite reflectance were also made. Rock-Eval in particular points to a maturation stage well within the oil window, less than 470°F. Why the reservoir produces both gas and oil is not understood at this time.

In essence, the quartz and feldspar silt content can be appreciable in these shales, and perhaps the term “mudstone” (incorporating both silt and clay) is more appropriate. Calcite is obviously present from the overall calcareous mudstone description. Much of the calcite is logically attributable to calcareous fossils including thin-shelled brachiopods,

*Table 1. Composite Geochemical Table**

Depth (feet)	TOC (wt. %)	S_1 (mg/g)	S_2 (mg/g)	S_3 (mg/g)	T_{max} (°F)	HI	OI	S_1/ TOC	PI	Calculated Ro
5876.4	1.17	0.49	1.07	0.30	461	92	26	42	0.31	1.14
5903.3	1.77	1.90	2.50	0.45	444	141	25	108	0.43	0.83
5930.4	1.39	1.49	2.12	0.56	442	152	40	107	0.41	0.80
6009.3	0.46	0.79	0.44	0.63	397	95	138	172	0.64	N/A
6017.5	0.05	0.03	0.10	0.23	473	193	453	60	0.24	1.35
6030.4	1.32	0.84	1.52	0.48	445	115	37	63	0.36	0.85
6036.6	0.78	0.97	0.74	0.52	432	95	67	124	0.57	0.62

*S_1 is the amount of free hydrocarbons (gas and oil) in the sample (in milligrams of hydrocarbon per gram of rock). If S_1 >1 mg/g, it may be indicative of an oil show. S_2 is the amount of hydrocarbons generated through thermal cracking of nonvolatile organic matter. S_2 is an indication of the quantity of hydrocarbons that the rock has the potential of producing should burial and maturation continue. S_3 = the amount of CO_2 (in milligrams CO_2 per gram of rock) produced during pyrolysis of kerogen. S_3 is an indication of the amount of oxygen in the kerogen. T_{max} is the temperature at which the maximum release of hydrocarbons from cracking of kerogen occurs during pyrolysis (top of S_2 peak). T_{max} is an indication of the stage of maturation of the organic matter. HI is the hydrogen index (HI = [100 x S_2]/TOC). OI is the oxygen index (OI = [100 x S_3]/TOC). PI is the production index (PI = S_1/[S_1 + S_2]).

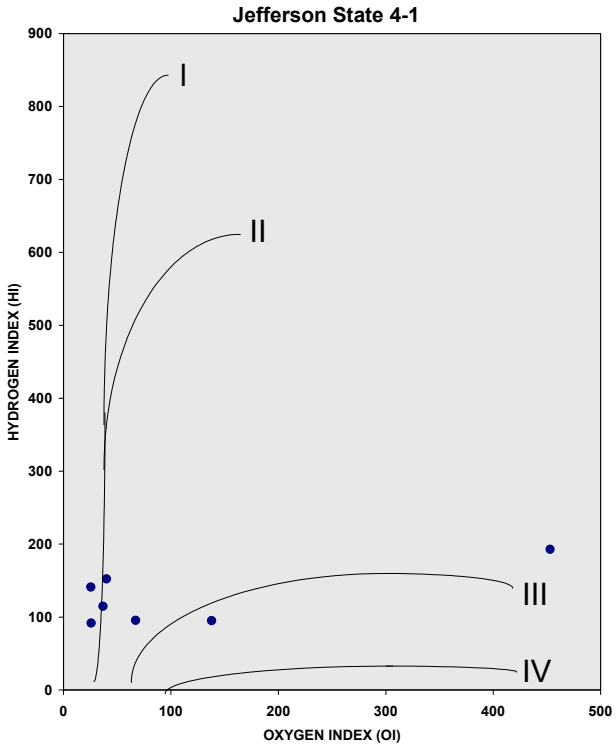

Figure 2. Kerogen type determination from TOC and Rock-Eval pyrolysis data. Types I and II will generate oil, type III gas and type IV little or no hydrocarbon.

pelecypods, ostracods, sponge spicules, microfossils, and much less common taxa (e.g. corals). Also, calcite occurs in diagenetic patches of various origins. The carbonate mineral of more variability from a quantitative perspective is dolomite or silty dolomite. This mineral likely ranges from a minor presence (less than 10%) to rocks that are nearly 100% dolomite - a compositional variability that is partly responsible for some of the wireline log variability seen for the three shale intervals or formations.

Microscopic work emphasized thin section work with photomicrographs of a series of plane and cross-polarized views implementing a traditional petrographic transmitted light source (Appendix B). In addition, several views result from an ultra-violet reflected light source using a blue-violet filter. The former transmitted light views allow identification of minerals, their grain size (to some degree for mudrocks), and compaction/cementation (diagenetic) effects upon the original sedimentary materials. In some cases, magenta epoxy can be seen from pores of some magnitude. The latter epifluorescent or reflected light views are qualitative estimates of porosity-only images, where pores usually are represented by light yellow green (mesopores) and orange (micropores) hues. In some cases, mineral fluorescence especially from dolomites (also yellow-green) can make porosity detection difficult.

Because of this potential confusion regarding mineral fluorescence versus porosity fluorescence, SEM techniques were used to verify the presence or absence of void space. Additionally, energy dispersive X-ray spectroscopy (EDAX) as explained in the SEM photomicrograph materials (Appendix C) can be utilized in detection of major atomic elements, thus allowing modest mineralogy detection for specific grains. Most certainly, SEM work was instrumental in void space determination particularly for the mudrocks (shales). It is certainly also true that SEM samples are extremely small and may not be completely reflective of overall reservoir characteristics.

NATURAL FRACTURES

Five generic types (or "classes") of natural fractures occur in these rocks:

1. short fractures of a vertical nature but are sinuous along their length,
2. microfractures are particularly developed in a carbonate facies of the Ismay, where rigid allochems are preferentially cracked,
3. filled and partially open, mostly subvertical fractures commonly located in the mechanically strong carbonates are stratigraphically proximal to the more ductile calcareous organic mudstones,
4. filled and partially filled subvertical cracks common to the mudstones themselves, some of which are proximal to carbonates and others which have no clear development attributable to contrasting mechanical properties, and
5. tension gash development associated with stylolitization.

The Jefferson State well was fractured on several scales (Appendix D). The first set (type 1 above) of a short and sinuous nature is likely comprised of syneresis cracks related to dewatering of soupy muds which later were occupied by solid mineral infill, mostly calcite and/or pyrite. The best examples occur in the Mule 31-K well at 5923.5 to 5925 feet (core depth). The microfractures (type 2) - related to perhaps differential compaction of allochems - occur in the oil-stained carbonates in the Jefferson State well between 6010.5 to 6016 feet (Appenidx D). The third type of carbonate cracking (type 3) is most impressive in the Mule dolostones or silty dolostones quite proximal to the underlying calcareous mudstones of the Chimney Rock (6097.5 to 6101.5 feet). The most impressive fractures in the mudstones themselves (type 4) occur in the Jefferson State well in the Gothic shale itself (Appenidx D). These cracks are partially to completely occluded by calcite mainly, and their origin remains a bit problematic. These cracks may simply be related to structural flexing. Type 5 development appears minor, and a good example of such cracks is situated in the Mule well at around 6097.5 feet in the carbonates above the Chimney Rock mudstones.

GEOLOGIC/GEOCHEMICAL RESULTS

All three shale units usually exhibit mud log shows while being penetrated. In fact, the Hovenweep and Gothic shales gave off significant gas shows while being cored in the Jefferson State well, and the Chimney Rock, while being drilled in the Jefferson State, also demonstrated significant evolved gas while being drilled. Porosity measurements of the Hovenweep and Gothic shales indicated modest porosities and permeabilities as seen in Table 2, and these laboratory numbers are considerably lower than other more commonly known gas productive shales (Barnett Shale of central Texas; Fayetteville

Table 2. Petrophysical Laboratory Measurements

Depth (feet)	As-Received Bulk Density (g/cm^3)	As-Received Grain Density (g/cm^3)	Dry Grain Density (g/cm^3)	Porosity (% BV)	Water Saturation (% of PV)	Gas Saturation (% of PV)	Mobile Oil Saturation (% of PV)	Gas-Filled Porosity (% of BV)	Bound Hydrocarbon Saturation (% of BV)	Bound Clay Water (% of BV)	Pressure-Decay Permeability (md)
5904.70	2.616	2.693	2.716	4.05	11.97	71.28	16.75	2.88	0.68	4.26	0.000070
5929.70	2.624	2.676	2.691	2.69	12.48	71.91	15.60	1.94	0.56	4.44	0.000064
6029.80	2.656	2.690	2.697	1.61	7.31	77.45	15.24	1.25	0.44	3.04	0.000057
6030.60	2.624	2.698	2.706	3.16	4.61	87.71	7.68	2.77	0.55	4.08	0.000065

Shale of Arkansas), when using the same type of analysis. It may simply be that the natural fractures common to the Gothic interval may be largely responsible for production. Details of production potential in terms of rock matrix characteristics can be adequately seen in the attached TRA (permeability, porosity, saturation), thin section photomicrographs, and SEM analyses.

Most of the observed matrix porosity is attributable to clay micropores in the mudrocks and to microintercrystalline porosity in the dolomite interbeds. In all cases, porosity is modest as determined from all three methods of study; however, one can see that the associated dolomites possess intercrystalline void space, a type of porosity usually conducive to some permeability potential. The porosity of these dolomites appears from a visual perspective, anywhere from 3 to 5%. Such resulting matrix permeability (unfortunately not measured directly in this study) is likely adequate for significant gas production. It also may be likely that the associated porous limestones, silty limestones, and sandstones provide additional production recoveries. Very little doubt exists however, that the mudstones or shales are instrumental in sustaining hydrocarbon production, both in terms of interstitial gas as well as desorbed gas from the organic material, especially as recognized in slabbed core, thin section, and SEM. In sum, the shale study may eventually point to a resource play, where all lithologies and natural fractures contribute to actual production.

In almost all cases, hydraulic fracturing of the mudstones themselves will likely access developments of natural fractures, and we feel that these cracks likely contribute to the permeability needed in this play. It should also be emphasized that the mudstones themselves have some gas-filled porosity (see Table 2) which would contribute to the production as well. Although desorptive effects are not known at this time, desorption of gas from the organic material (TOC) in the mudstones will also likely be a third factor in assessing the production mechanism – and quantification of the relative volumes of free gas and desorbed gas can be relevant to production simulations.

It is quite likely that formation sensitivity is a real problem here, based in part on the geological investigations. The small pore sizes of both the mudstones and dolomites are likely to be susceptible to damage related to drilling and completion fluids. At this time, we do not know whether the intervals are overpressured, underpressured, or normally pressured, but underpressuring might make the formations vulnerable to gelled fluids, similar to the problems encountered by the underpressured Lewis Shale of northwestern New Mexico. Because of the clay content of the shales themselves, containing both significant amounts of chlorite and lesser quantities smectite in proximity to available void space, use of hydrochloric acid and fresh water respectively could pose serious problems. Operators might instinctively want to try HCl in what is “normal” to a carbonate basin, but such acid treatments on iron-rich chlorite (and pyrite) could be disastrous in terms of creating significant amount of insoluble iron hydroxides, which would occlude the small pores even further (even with chelation or similar iron control additives). The potential for damaging effects of fresh water on the small amounts of smectite is a borderline call based on current knowledge, but such damage is certainly possible - care should be exercised here until smectite abundance is better characterized through more X-ray diffraction (XRD) testing. Up to this point, we have conducted only two such tests although SEM work has spotted some smectite indeed lurking near the small pores, especially in the dolomite interbeds. Please consult the XRD (Appendix E) and SEM (Appendix C) results.

MECHANICAL PROPERTIES

Triaxial Compression Testing

The results of triaxial compression measurements on horizontal samples from the Jefferson State 4-1 core are shown in Table 3. In addition to the static mechanical properties shown in Table 3, ultrasonic wave velocities were measured using standard transmission techniques. Elastic formulae were further used to calculate the dynamic mechanical properties (Table 4).

These laboratory data were used to calibrate logging data. Figure 3 shows logging and laboratory predictions of Poisson's ratio. No correction was made for Poisson's ratio. Figure 4 compares the static and logging values. However, for Young's modulus, as is always the case, dynamic values of the modulus are overestimates. Static values are required for completion design.

Figure 5 shows the characteristic comparison between static and dynamic values for Young's modulus – logging values are dynamic and a correction needs to be applied. The relationship used a linear combination of the gamma ray count (GAPI) and the apparent matrix density (g/cm^3).

$$\frac{E_{static}}{E_{dynamic}} = 3.364699503 + 0.004385682 \times GR - 1.04726626 \times DENSMA$$

Figure 6 shows the synthesized values of static Young's modulus and the laboratory measurements used to correct the raw dynamic values.

While modulus calibrations are common and there is some fundamental basis for them, forecasting in-situ strength has less basis and is usually done strictly on the basis of correlations with existing logging data. A common approach is to adopt relationships shown by Deere and Miller (1966). In this case, the measured strength data were compared with various linear combinations of logging data. For whatever reason, the relationship between in-situ strength and sonic porosity was the best (albeit improvement is merited) fit. The strength-porosity relationship used is shown in Figure 7 and the vertical profile of in-situ strength is shown in Figure 8.

These are very strong zones. Often, the potential for fracturing is correlated to the degree of brittleness of the rock. One measure of this is the amount of energy released when failure occurs. This was approximated as follows.

Table 3. Summary of Triaxial Compression Tests from the Jefferson State 4-1 core.

Depth (ft)	As-Received Bulk Density (g/cm^3)	Effective Confining Pressure* (psi)	Effective Compressive Strength (psi)	Effective Residual Compressive Strength (psi)	Quasi-Static Young's Modulus (psi)	Quasi-Static Poisson's Ratio
5876.2	2.672	3526	38,546	15,891	8,211,000	0.29
5903.7	2.613	3610	24,130	18,435	5,945,000	0.24
5930.0	2.636	3558	25,783	19,563	5,593,000	0.25
6009.6	2.656	3606	38,181	17,976	6,402,000	0.31
6017.3	2.720	3610	36,350	22,075	6,962,000	0.33
6030.0	2.652	3618	42,263	20,543	7,592,000	0.25
6036.5	2.663	3622	45,092	26,227	7,332,000	0.24

*Pore pressure = 0 psi in all tests.

Table 4. Dynamic Mechanical Properties Determined During Triaxial Compression Testing.

Sample ID Depth (ft)	Axial Stress Difference (psi)	Effective Confining Pressure* (psi)	Effective Mean Stress (psi)	Test Bulk Density (g/cm^3)	P-Wave Velocity (ft/s)	S-Wave Velocity (ft/s)	Poisson's Ratio	Young's Modulus (10^6 psi)	Bulk Modulus (10^6 psi)	Shear Modulus (10^6 psi)
BA-1 5876.2	5	3526	3528	2.678	19,363	10,515	0.29	10.300	8.208	3.989
	5753		5445	2.679	19,566	10,551	0.30	10.406	8.461	4.018
	14,518		8366	2.680	19,779	10,601	0.30	10.538	8.717	4.058
	20,906		10,495	2.681	19,904	10,627	0.30	10.611	8.871	4.079
	27,808		12,796	2.681	19,930	10,626	0.30	10.618	8.912	4.079
	33,565		14,714	2.682	19,862	10,600	0.30	10.565	8.843	4.061
	12,348		7642	2.668	18,790	10,003	0.30	9.369	7.896	3.597
BA-5 5903.7	0	3610	3609	2.622	17,062	10,067	0.23	8.830	5.512	3.581
	5647		5493	2.624	17,077	10,070	0.23	8.843	5.529	3.585
	12,094		7642	2.625	17,162	10,068	0.24	8.873	5.637	3.585
	18,054		9628	2.626	17,211	10,062	0.24	8.887	5.704	3.582
	20,458		10,429	2.625	17,231	10,050	0.24	8.876	5.738	3.573
	14,818		8549	2.645	16,731	9837	0.24	8.526	5.379	3.450
BA-8 5930.0	3	3558	3559	2.647	17,232	10,039	0.24	8.938	5.800	3.595
	4291		4988	2.648	17,293	10,053	0.24	8.978	5.863	3.606
	16,071		8915	2.651	17,400	10,060	0.25	9.029	5.994	3.614
	18,774		9816	2.651	17,426	10,058	0.25	9.036	6.029	3.614
	21,193		10,622	2.651	17,450	10,055	0.25	9.039	6.063	3.611
	15,893		8855	2.634	17,162	9928	0.25	8.736	5.791	3.499
	15,279		8651	2.633	17,175	9923	0.25	8.730	5.807	3.494
BA-12 6009.6	4	3606	3607	2.676	19,142	10,538	0.28	10.270	7.872	4.004
	4295		5037	2.677	19,575	10,693	0.29	10.618	8.322	4.124
	12,996		7938	2.678	19,598	10,720	0.29	10.671	8.333	4.147
	20,631		10,483	2.679	19,620	10,679	0.29	10.618	8.407	4.117
	30,428		13,748	2.679	19,493	10,568	0.29	10.414	8.339	4.030
	34,438		15,085	2.676	19,692	10,568	0.30	10.452	8.613	4.027

Table 4 continued.

Sample ID Depth (ft)	Axial Stress Difference (psi)	Effective Confining Pressure* (psi)	Effective Mean Stress (psi)	Test Bulk Density (g/cm^3)	P-Wave Velocity (ft/s)	S-Wave Velocity (ft/s)	Poisson's Ratio	Young's Modulus (10^6 psi)	Bulk Modulus (10^6 psi)	Shear Modulus (10^6 psi)
BA-13 6017.3	2	3610	3610	2.809	20,577	11,013	0.30	11.930	9.905	4.591
	6003		5611	2.810	20,874	11,139	0.30	12.226	10.235	4.699
	11,198		7342	2.811	20,961	11,223	0.30	12.397	10.282	4.772
	18,968		9932	2.812	21,146	11,298	0.30	12.578	10.494	4.837
	25,340		12,056	2.812	21,122	11,286	0.30	12.550	10.470	4.826
	28,411		13,080	2.811	21,050	11,205	0.30	12.386	10.442	4.756
	18,462		9764	2.733	18,975	9725	0.32	9.206	8.615	3.482
BA-15 6030.0	4	3618	3619	2.656	18,501	10,874	0.24	10.462	6.608	4.232
	7033		5962	2.658	18,567	10,878	0.24	10.497	6.694	4.237
	15,070		8641	2.659	18,631	10,869	0.24	10.513	6.794	4.232
	21,185		10,680	2.660	18,615	10,869	0.24	10.512	6.774	4.234
	29,055		13,303	2.661	18,676	10,856	0.24	10.522	6.873	4.226
	37,430		16,094	2.663	18,644	10,823	0.25	10.474	6.870	4.203
	16,816		9223	2.655	18,065	10,270	0.26	9.519	6.644	3.774
BA-19 6036.5	4	3622	3624	2.668	18,420	10,165	0.28	9.519	7.245	3.715
	4918		5262	2.669	18,546	10,181	0.28	9.576	7.401	3.728
	10,928		7265	2.671	18,622	10,189	0.29	9.610	7.497	3.735
	18,831		9899	2.672	18,648	10,190	0.29	9.624	7.536	3.738
	26,802		12,556	2.673	18,719	10,180	0.29	9.632	7.644	3.733
	35,244		15,371	2.675	18,539	9845	0.30	9.110	7.730	3.494
	23,016		11,295	2.645	18,194	9650	0.30	8.657	7.373	3.319

*Pore pressure = 0 psi in all tests.

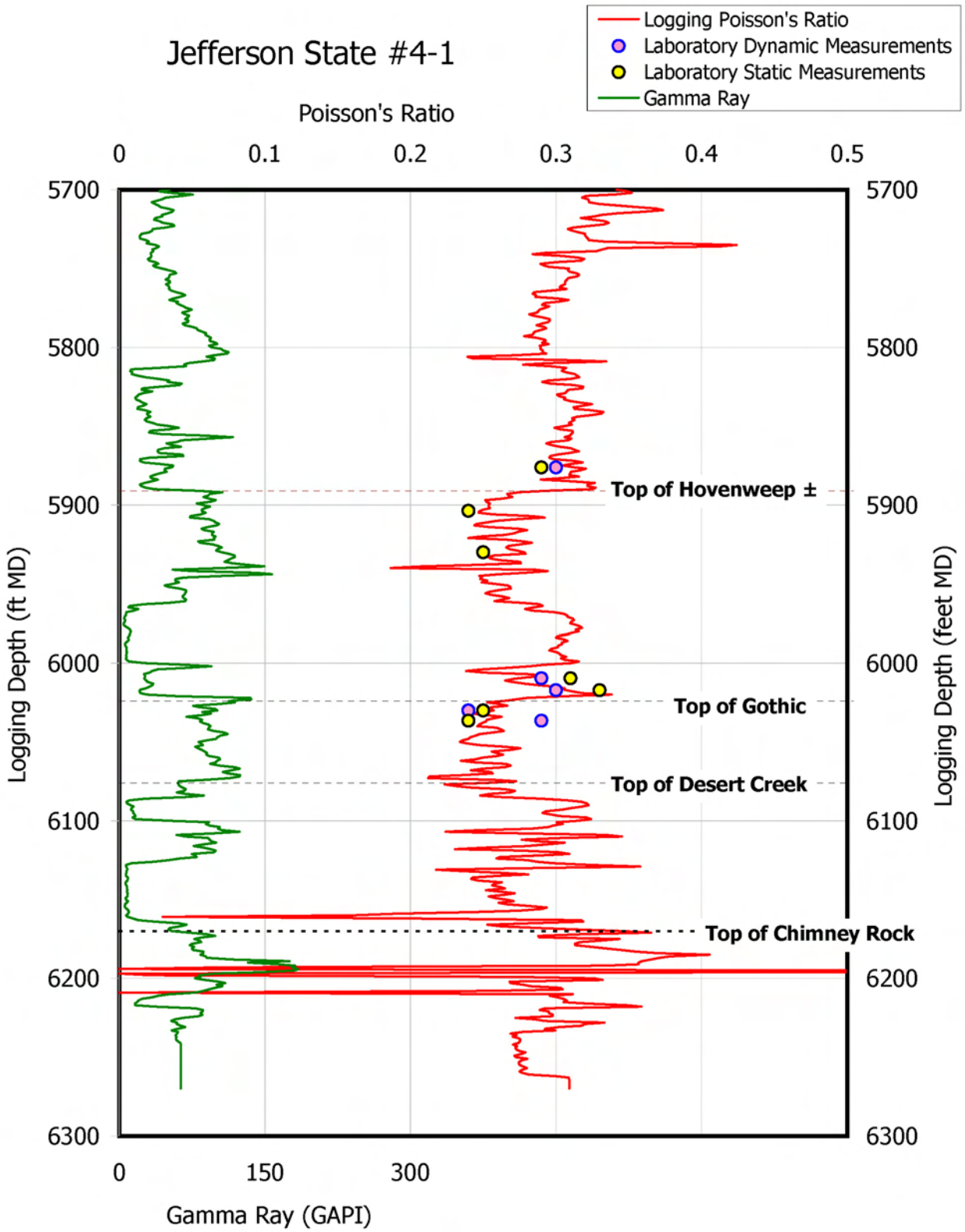

Figure 3. Variation of laboratory and logging-predicted values for Poisson's ratio.

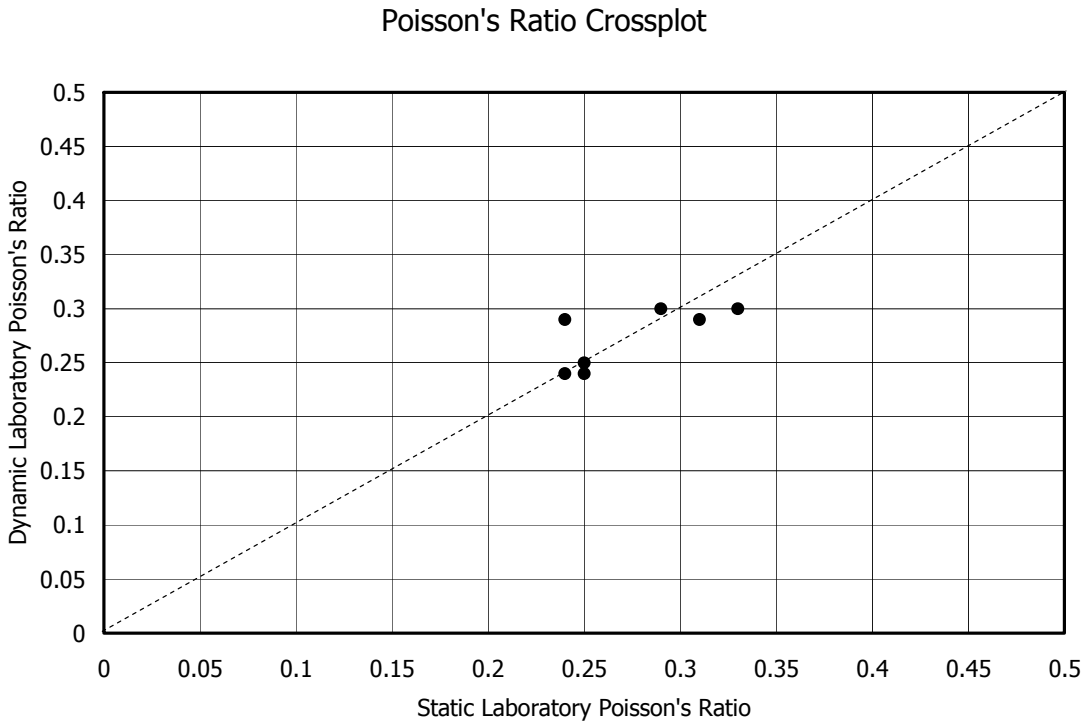

Figure 4. Variation of static and dynamic (ultrasonic) laboratory values for Poisson's ratio.

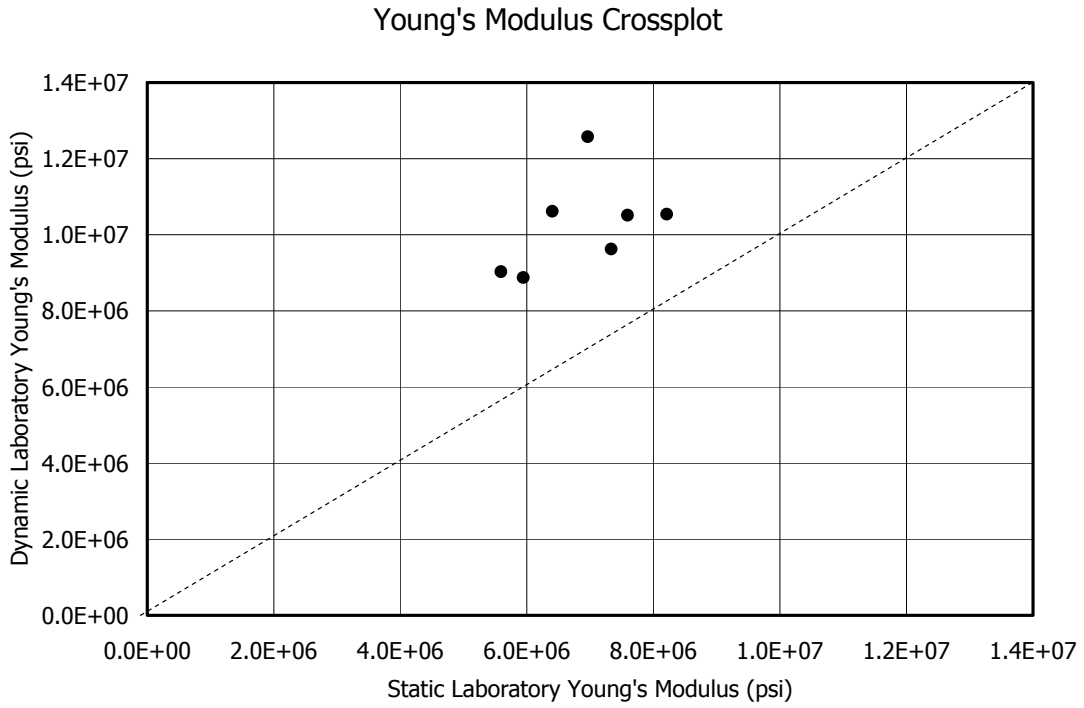

Figure 5. Variation of static and dynamic (ultrasonic) laboratory values for Young's modulus.

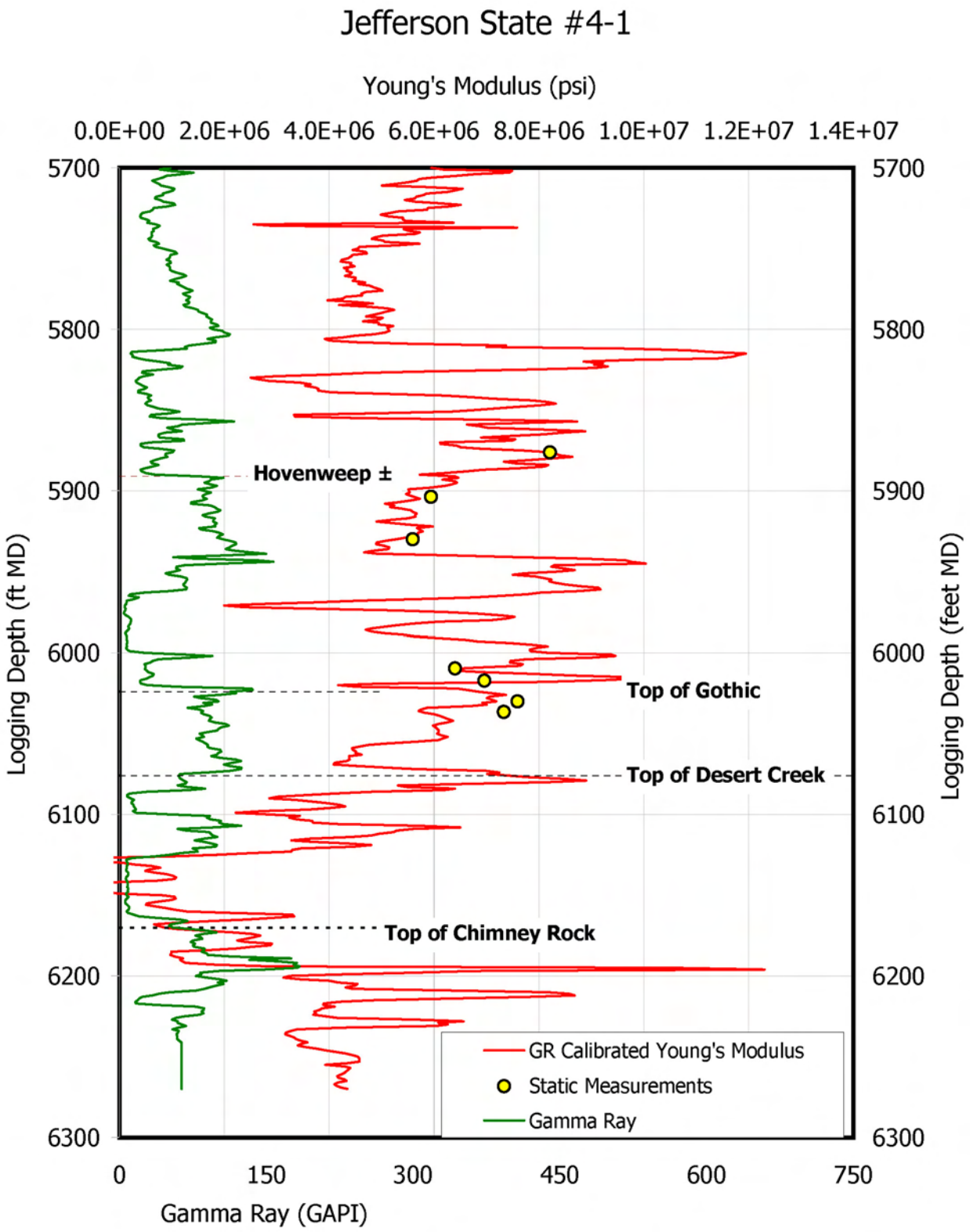

Figure 6. This figure shows calibrated logging values for Young's modulus and the discrete laboratory measurements that were used for the calibration. After attempting numerous multiparameter correlations, it was determined that the best calibration relationship for Young's modulus used GR and DENSMA.

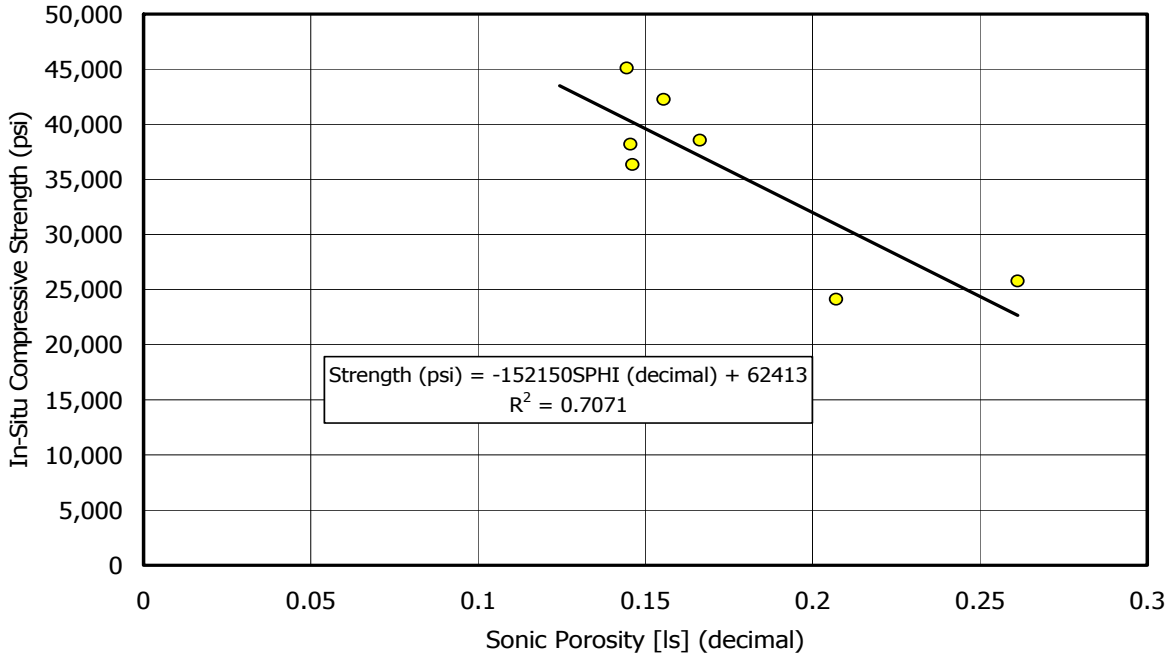

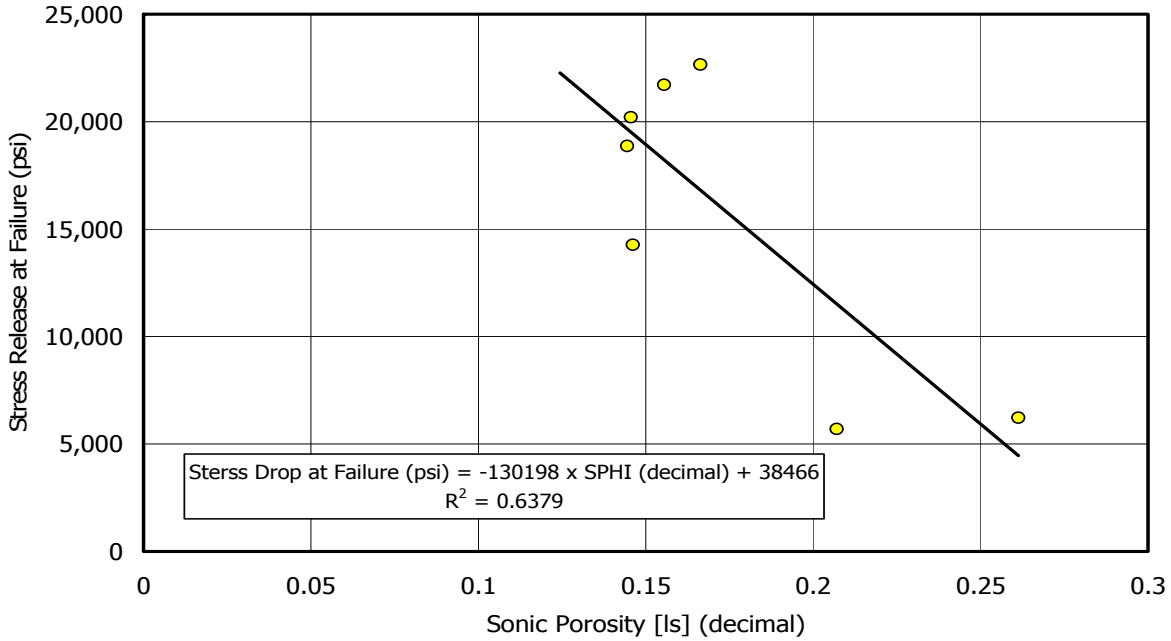

Figure 7. These two panels show laboratory measured data (the in-situ compressive strength, and the stress drop at failure) plotted against the sonic porosity with an annotation of linear regression fits. After attempting numerous multiparameter correlations, it was determined that the best calibration relationship for an estimate of in-situ strength used the sonic porosity (top panel). Similarly the bottom panel shows a prediction of how much stress drop occurs at failure – this was part of a relationship showing energy stored in the material – an indicator of the degree of brittleness.

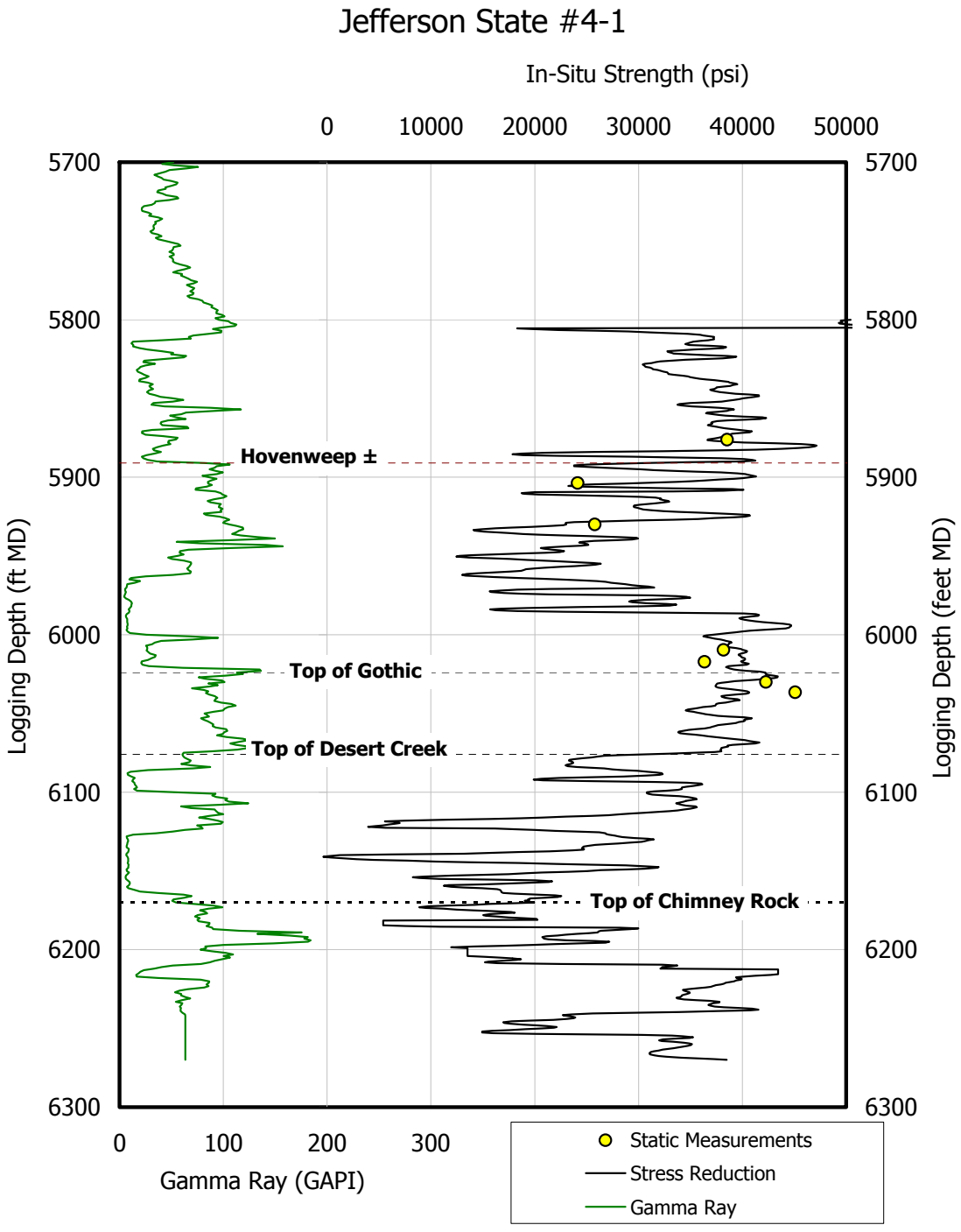

Figure 8. Logging inference of in-situ strength (triaxial compression on as-received horizontal plugs with an effective confining pressure of 0.6 psi/ft was used to calibrate the data). Calibration was based on the sonic porosity.

1. Approximate the stress drop on failure as the difference between the peak and the residual triaxial strengths, calibrated based on the sonic porosity (Figure 8)
2. Grossly approximate the energy released (alternatively view this as energy stored with potential for fracturing) as follows ["C" denotes the triaxial compressive strength, either peak or residual):

$$Energy \propto 0.5 \frac{C_{peak}}{E}\left(C_{peak} - C_{residual}\right)(1-2\nu)$$

This energy analog is plotted in Figures 9 and 10. The speculation is that the greatest fracture potential is where the stored energy is highest – in the Gothic. There is general agreement between predicted fracture potential and with the coregraphs and this approach seems like it could evolve to be a useful predictive tool.

Figure 11 is also an uncalibrated estimate of the in-situ stresses, using a conventional Eaton (1969)-type relationship.

CONCLUSIONS AND POSSIBLE FUTURE WORK

Conclusions

- The three shale intervals are indeed gas productive in certain areas.
- The porosity of all reservoirs is indeed modest - estimated based on testing at between 2 and 5%.
- The interbedded dolomite within and bounding the mudstone sections may be the most permeable conduit for sustained hydrocarbon production. Permeability is likely modest but appears best developed in intercrystalline porosity from euhedral to subhedral dolomite crystal aggregates.
- The larger partially filled natural fractures, filled mainly by calcite, could assist in providing a respectable initial production (IP) especially when the hydraulic fracturing protocol is able to access natural fractures. Much of this fracturing occurs in the associated dolomites although not exclusively.
- The calcareous mudstones are likely productive as well although matrix permeability is still in the nanodarcy range. Production from the mudstones is possibly related to both interstitial and desorbed gas.
- Although conclusions are decidedly preliminary, these Pennsylvanian "black shale" units from the Paradox Basin are likely another representation in a series of emerging resource plays.

Future Work

- More detailed work on fluid compatibility related to reservoir pressure, small pore sizes, and mineralogy.
- Understanding why gas production seems especially common to oil-prone reservoirs as indicated by the geochemical work done thus far.
- More detailed sampling and comprehension of the associated dolomites, and other carbonates/ clastics known to exist in stratigraphic proximity, to any hydraulic fracture treatment imposed on the shales/ mudstones themselves.
- More careful attention to possible stimulation methods and to the possibility of horizontal drilling (stimulated and unstimulated).
- More rock mechanics work on the

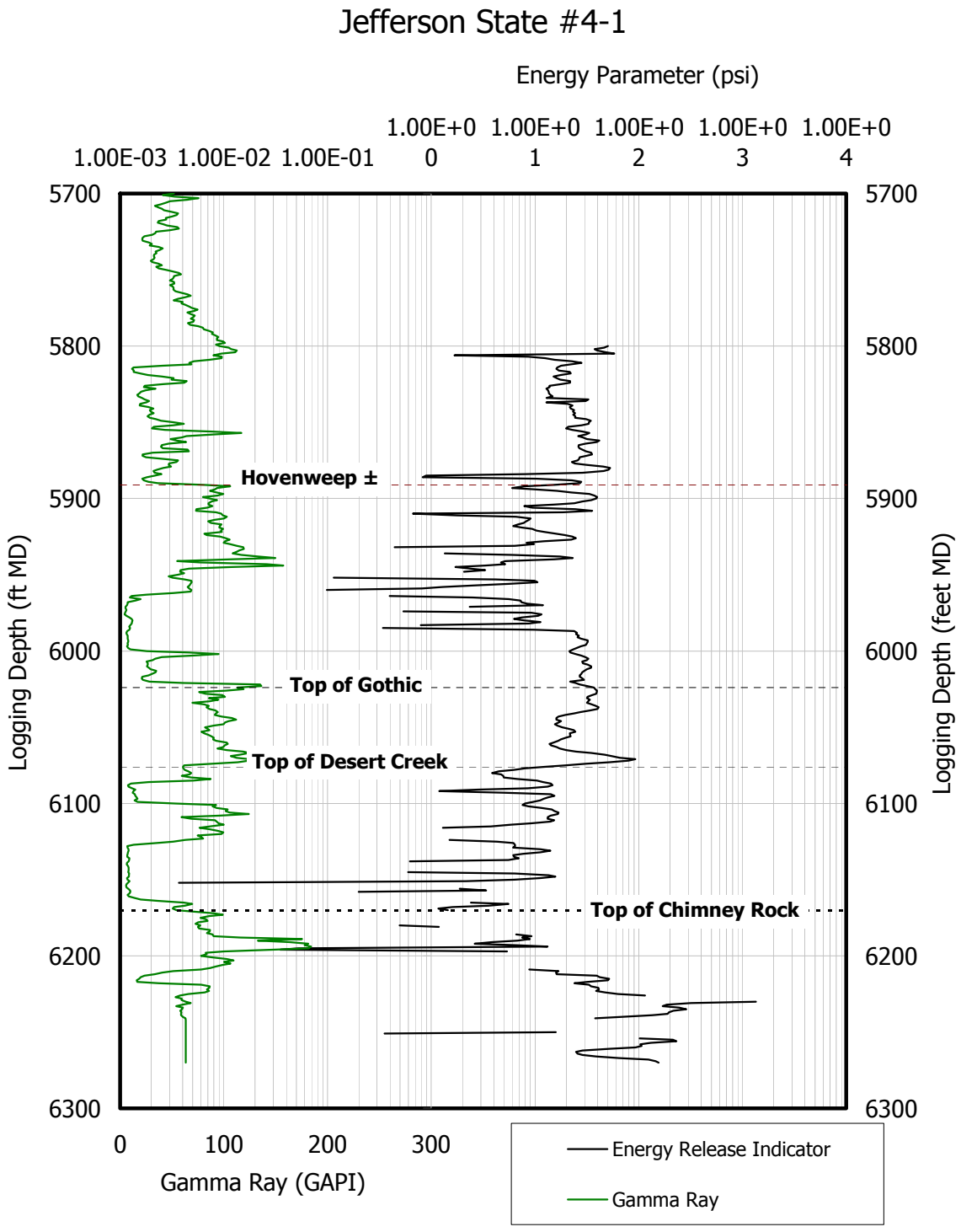

Figure 9. Logging inference of brittleness – based on estimates of stored energy. It is hypothesized and supported to some extent by the core logs that the higher the stored energy, the greater the potential for fracturing, shear, extensional or flexural during previous history.

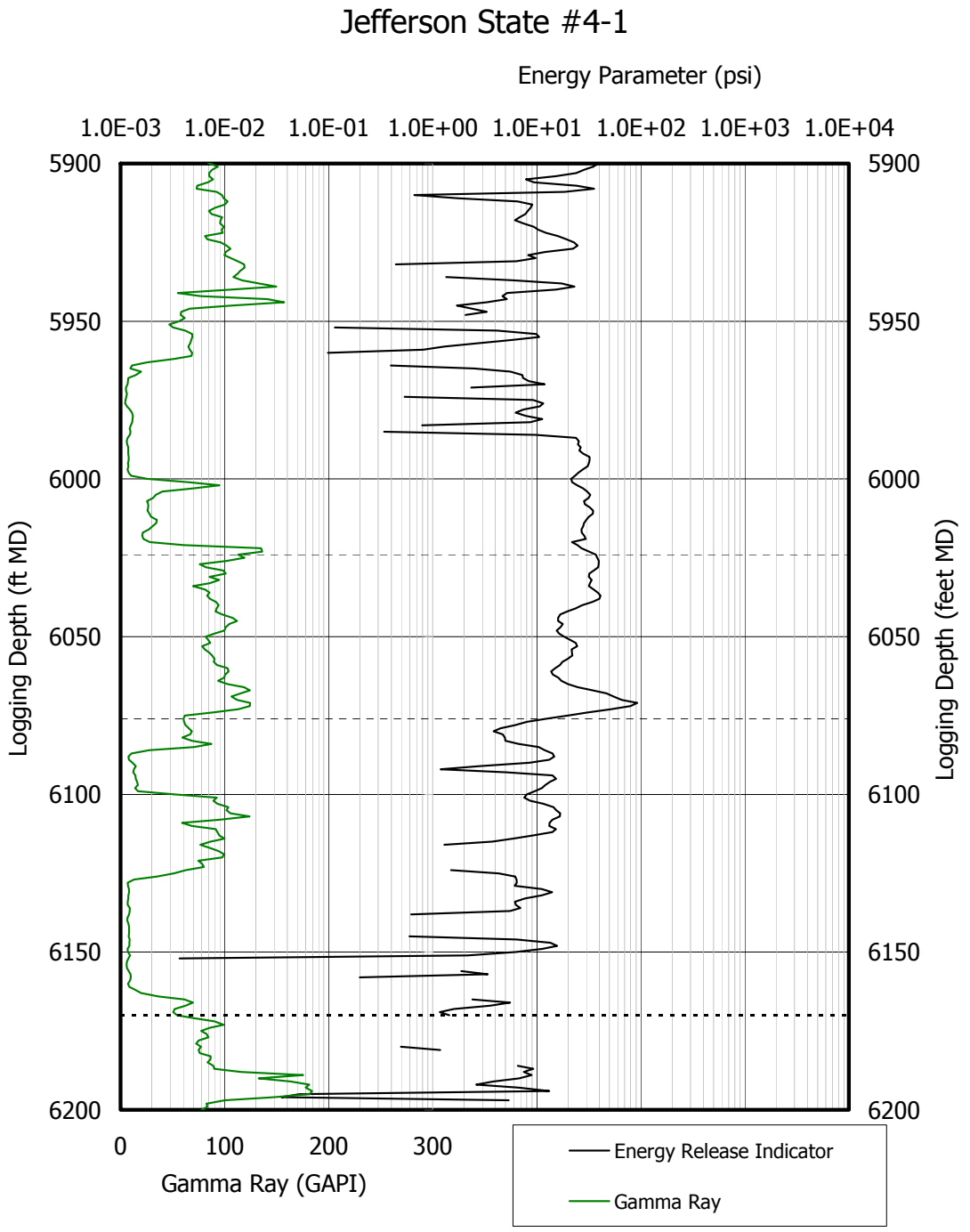

Figure 10. Expanded view of the Gothic shale - logging inference of brittleness – based on estimates of stored energy. It is hypothesized and supported to some extent by the core logs that the higher the stored energy, the greater the potential for fracturing, shear, extensional or flexural during previous history.

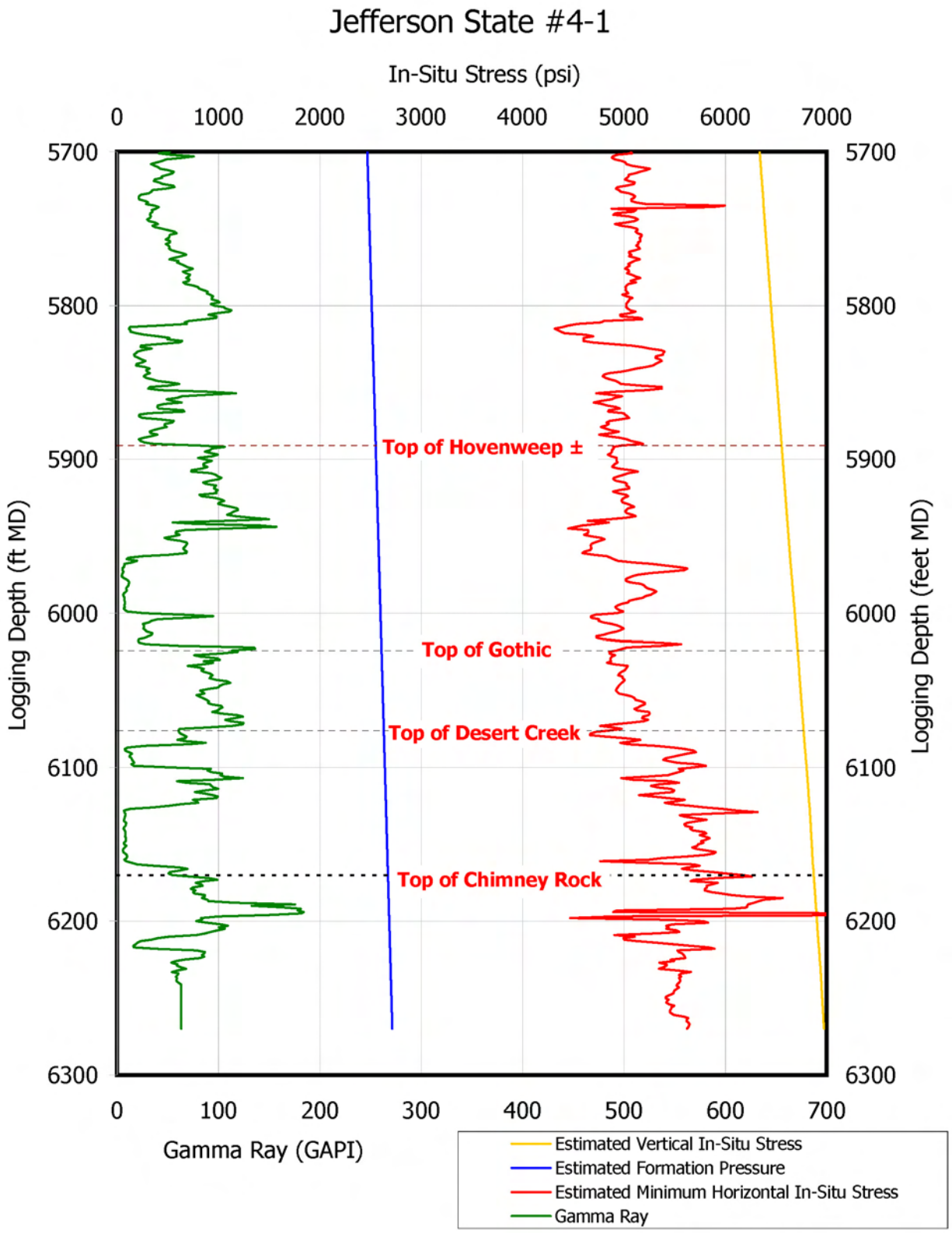

Figure 11. This figure shows the vertical variation in the minimum horizontal stress (which controls vertical growth of hydraulic fractures), the vertical stress (which is commonly used in logging estimates of the minimum horizontal stress), and the inferred formation pressure. Stresses were estimated using logging relationships and experience – corroborating evidence was not available.

mudstone-associated strata—especially on the limestones and dolostones—the goal is optimization of stimulation design.

- More petrophysical correlation and calibration of complex rock types are needed as part of the formation evaluation process—the goal is improved log interpretation.

REFERENCES

Deere D.U., and Miller, R.P.: *Engineering Classification and Index Properties for Intact Rock*, Air Force Weapons Laboratory Technical Report AFWL-TR-65-116, 1966, 277 p.

Eaton, B.A.: "Fracture Gradient Prediction and Its Application in Oilfield Operations," SPE 2163, Journal of Petroleum Technology, Volume 21, Number 10, October 1969, pp. 1353-1360.

Harr, C,L.: "Paradox Oil and Gas Potential of the Ute Mountain Ute Indian Reservation," in Geology and Resources of the Paradox Basin, Utah Geological Association Guidebook 25, Huffman, A.C. Jr., Lund, W.R., and Godwin, L.H. (ed), Salt Lake City, UT, 1996.

Appendix A – CoreGraphs

Core Description

2008-03-19

Well: Jefferson State 4-1 Company: Crownquest Oper.

Location: San Juan Co., UT Depth: 5899-5944 feet

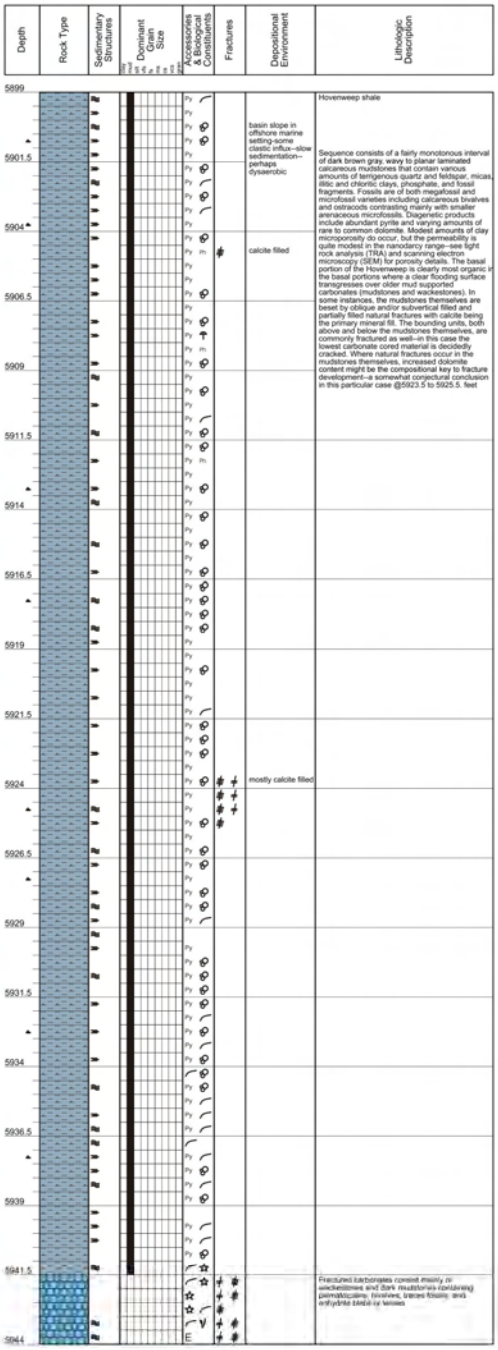

Legend

- Mudstone
- Shale or Mudstone-Calcareous
- Wackestone

V	Bioturbated		Partially Filled Vertical Fracture
	Carbonaceous	☆	Pelmatozoan
	Dolomitic or Ankeritic	Py	Phosphatic
E	Evaporitic		Planar Lamination
	Filled Vertical Fracture	Py	Pyritic
	Microfossil		Shell Fragment
			Wavy Lamination

Core Description

2008-03-19

Well: Jefferson State 4-1 Company: Crownquest Oper.

Location: San Juan Co., UT Depth: 6003-6041.5 feet

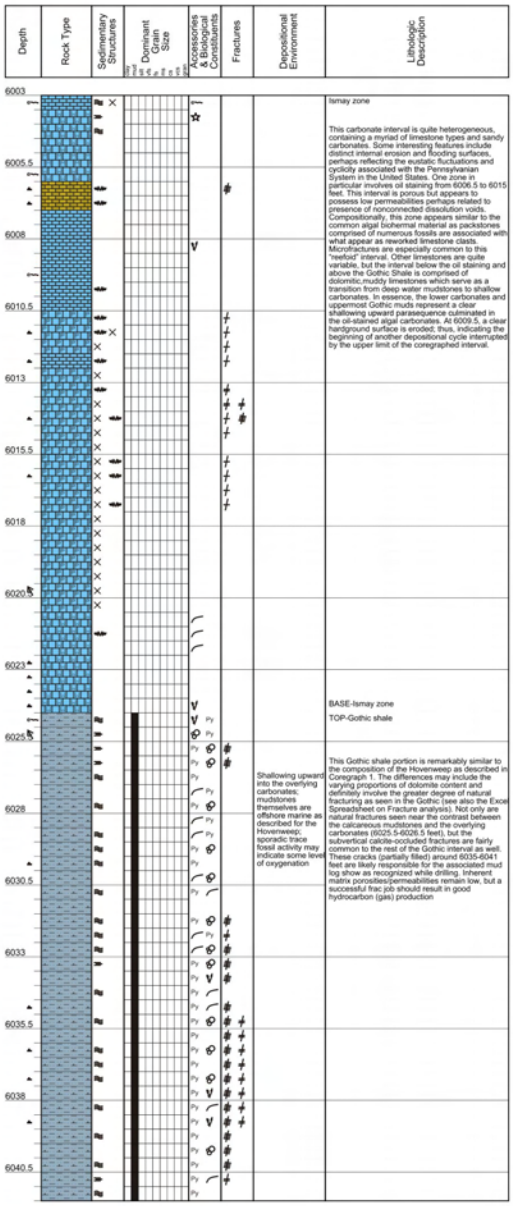

Legend

- Limestone
- Mudstone
- Packstone
- Sandy Limestone
- Shale or Mudstone-Calcareous
- Wackestone

- Bioturbated
- Coarsening Upward
- Dolomitic or Ankeritic
- Erosion Surface
- Filled Vertical Fracture
- Microfossil
- Open Vertical Fracture
- Partially Filled Vertical Fracture
- Pelmatozoan
- Planar Lamination
- Pyritic
- Rip-Up or Breccia Clast
- Shell Fragment
- Stylolitic
- Wavy Lamination

Core Description

2008-03-19

Well: Mule 31-K-1 Company: Harken Energy

Location: San Juan Co., UT Depth: 5900-5926

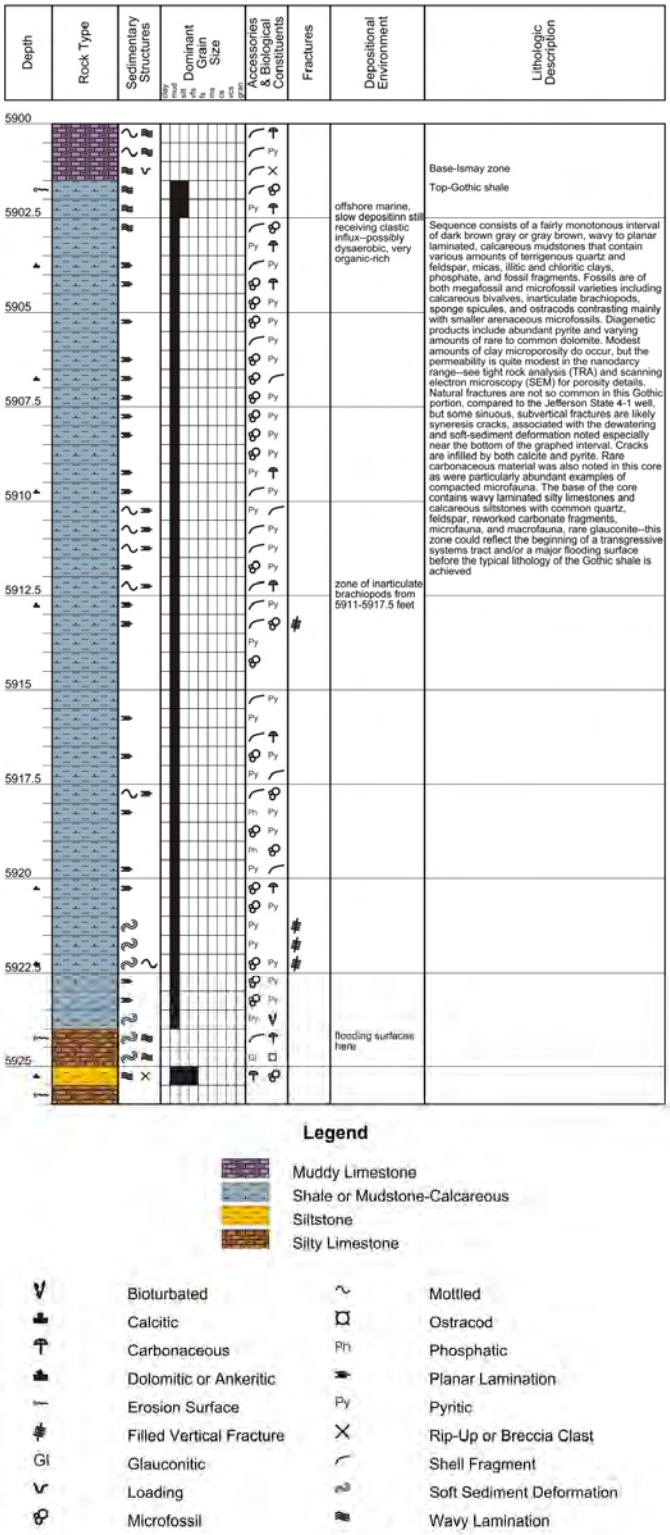

Core Description

2008-03-19

Well: Mule 31-K-1 Company: Harken Energy

Location: San Juan Co., UT Depth: 6095-6118 feet

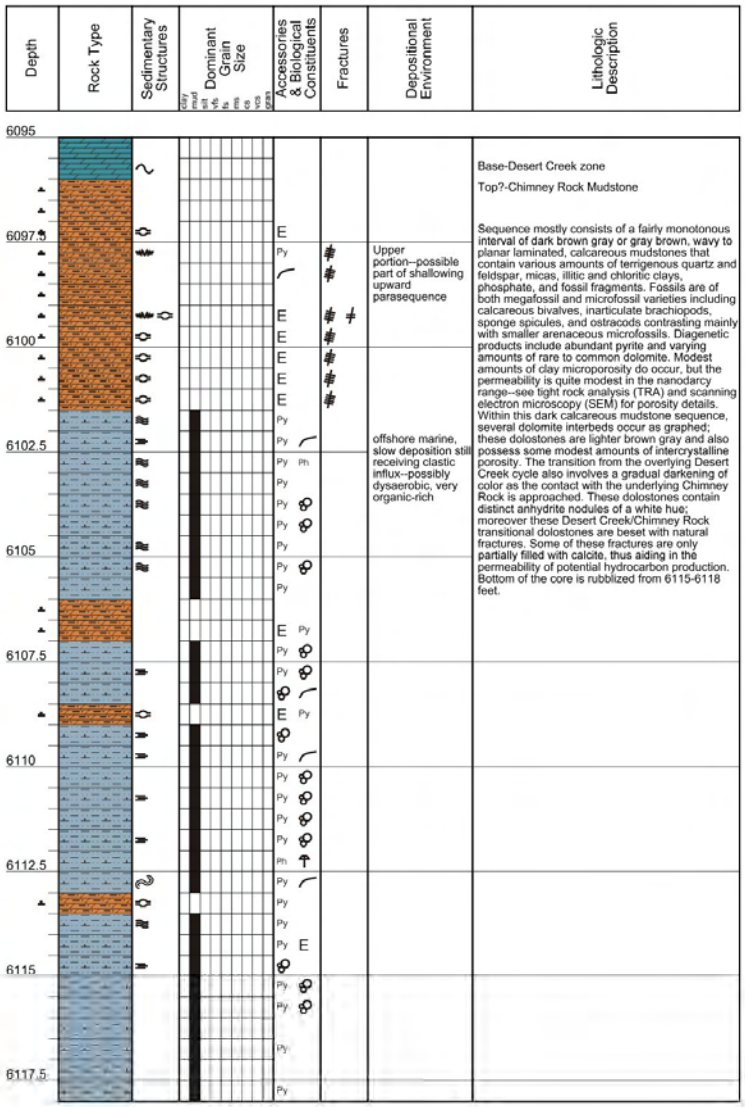

Legend

Dolomite
Shale or Mudstone-Calcareous
Silty Dolomite

	Calcitic		Partially Filled Vertical Fracture
	Carbonaceous	Ph	Phosphatic
E	Evaporitic		Planar Lamination
	Filled Vertical Fracture	Py	Pyritic
	Microfossil		Shell Fragment
	Mottled		Soft Sediment Deformation
	Nodular		Stylolitic
			Wavy Lamination

Appendix B - Thin Section Analysis

Jefferson State 4-1 5930.8 ft

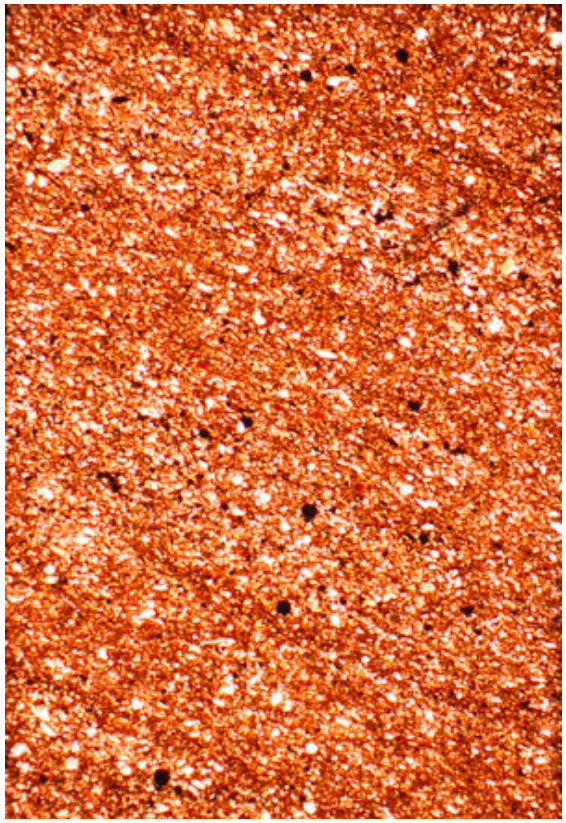

Depth: 5930.8 feet. Low magnification view of Hovenweep mudstone quite typical of most mudstones in these Pennsylvanian deposits. Terrigenous clastics are white here, pyrite and carbonaceous material appear black, clays and carbonates are brownish at this magnification. Plane-polarized light (40x).

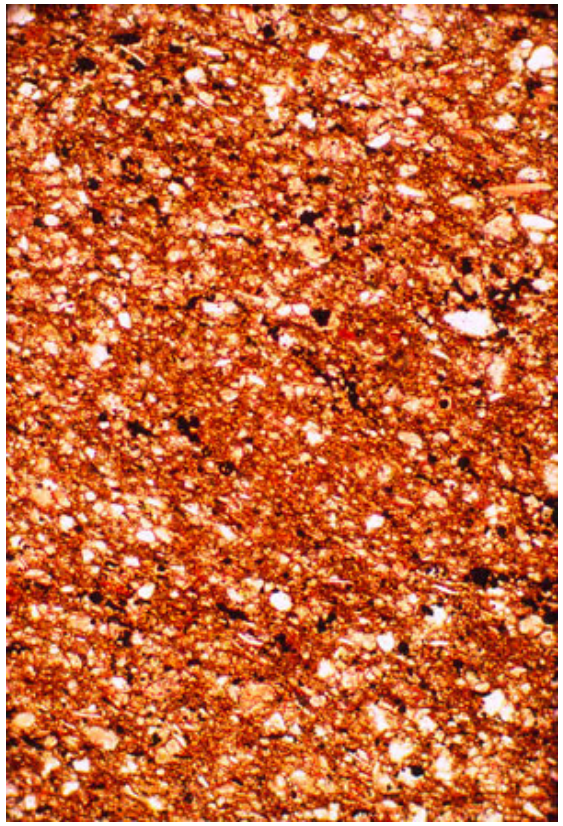

Depth: 5930.8 feet. Closer view of the above provides details of the textural elements. Influence of clastic debris is clearly apparent here, and the carbonate material, not clearly revealed in this view, indicates a decidedly mixed framework grain content. Plane-polarized light (100x).

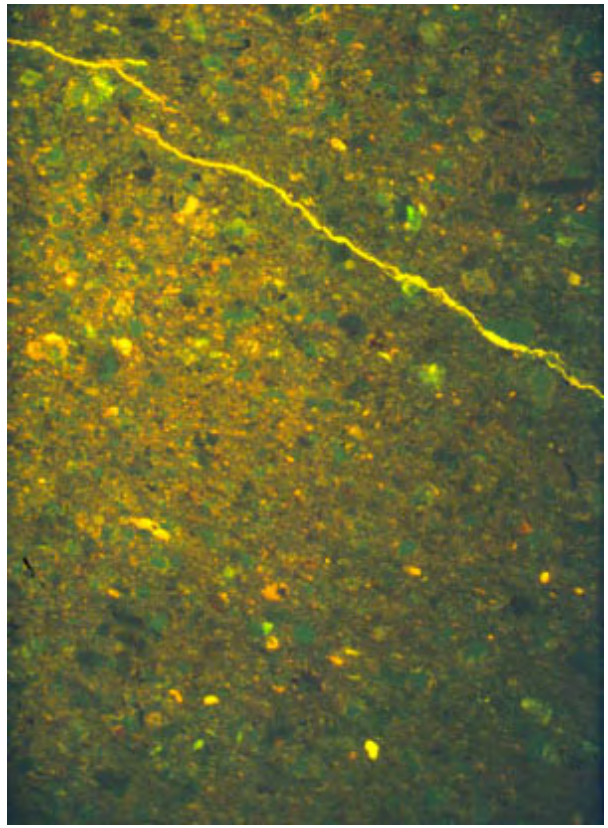

Depth: 5930.8 feet. Reflected ultra-violet light demonstrates a porosity only image, and most micropores appear orange in this view. This reflected light techniques only demonstrates the presence of pores and has no validity in predicting their quantitative occurrence. Epifluorescent light with blue-violet filter (100x).

Jefferson State 4-1 5948.4 ft

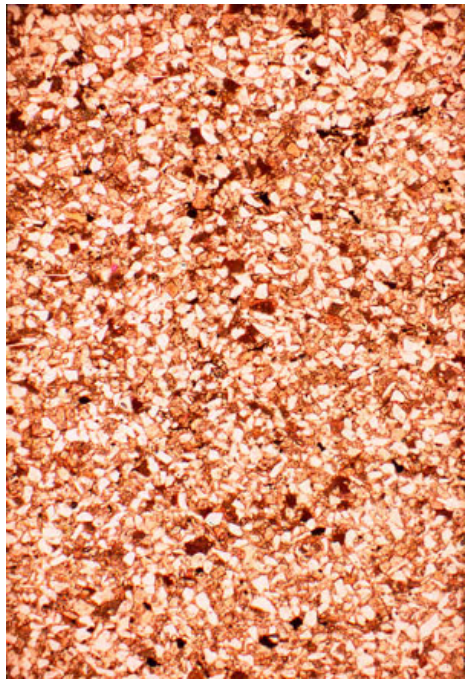

Depth: 5948.4 feet. Although this sample was not placed on the Jefferson State coregraph, this example is merely eight feet beneath the lowest bed of the Hovenweep Shale. Here, one can see a calcareous, muddy sandstone that may be affected by any hydraulic fracture treatment. This view appears to indicate a lack of porosity due to the absence of magenta-dyed epoxy. Plane-polarized light (40x).

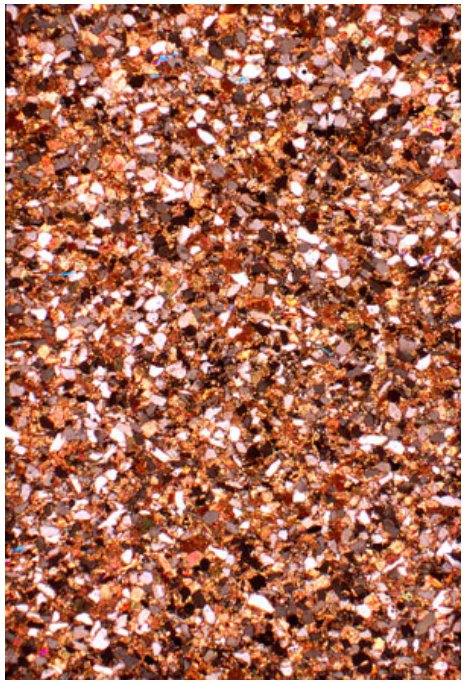

Depth: 5948.4 feet. The birefringent contrast in this cross-polarized view demonstrates the composition of both terrigenous clastics (appearing white), mica (blue flecks near top), and carbonate minerals (bronze hues). Some of the carbonate material is calcite and some is dolomite--thus a "mixed rock" geological designation is appropriate. No magenta epoxy is visible using this type of transmitted light. Cross-polarized light (40x).

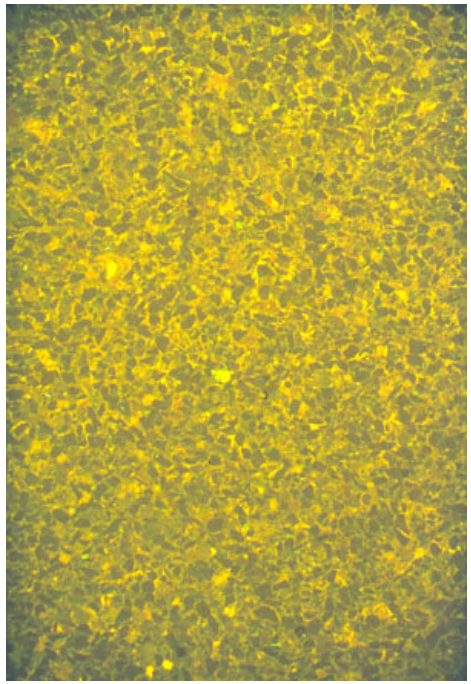

Depth: 5948.4 feet. Epifluorescent light of the above reveals porosity presence especially in the orange hues. Other fluorescence of the light yellow-green variety is mineral fluorescence, particularly from dolomite crystals. The point of showing this sample serves to illustrate the likelihood that nearby shale associated strata will possibly contribute to hydrocarbon production if affected by any stimulation treatment. Epifluorescent light with blue-violet filter (40x).

Jefferson State 4-1 - 6036.6 ft

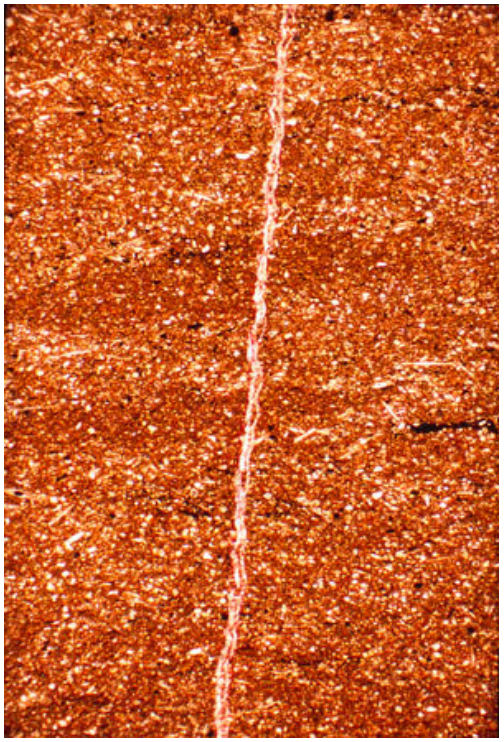

Depth: 6036.6 feet. An example of the underlying Gothic shale is also composed of terrigenous material, fossils, and clays. Mottled appearance may be related to some bioturbation. In this well, the Gothic is decidedly fractured, and in this view a subvertical fracture is composed of red-stained calcite. Not all fractures in this interval are completely occluded by diagenetic minerals--see appended fracture summary. Plane-polarized light (40x).

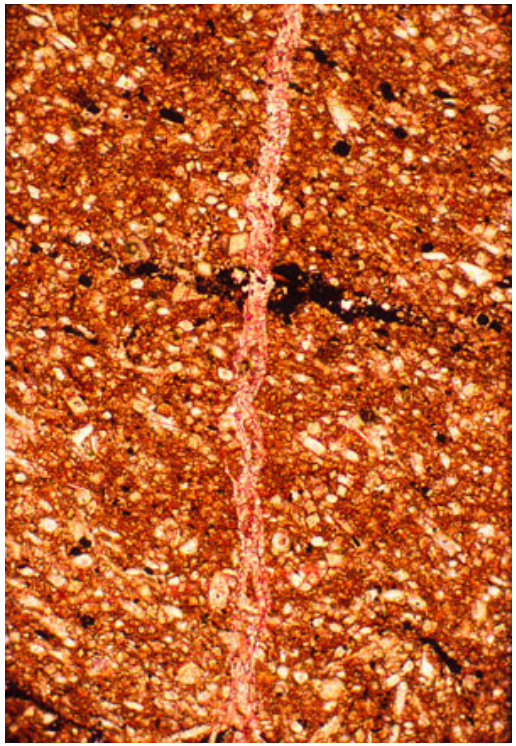

Depth: 6036.6 feet. Higher magnification illustrates the mixed mineralogy/grain content, the ribbon-like nature of the calcitic (red) fracture filling, and the dark material representing both carbonaceous material and pyrite. While an epifluorescent view of this sample is not provided, the mud matrix is indeed modestly microporous. Plane-polarized light (100x).

Mule 31-K – 5924.2 ft

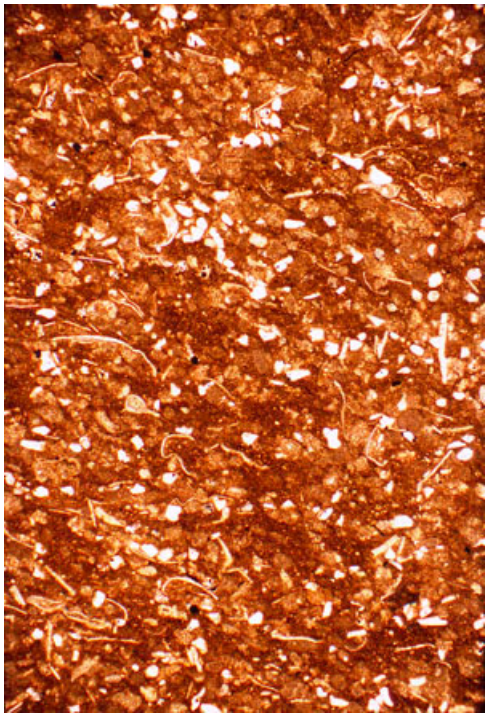

Depth: 5924.2 feet. Just below the base of the Gothic shale from the Mule well, this view demonstrates a little variability in that brachiopod and ostracod fragments are a bit more common here although terrigenous quartz and feldspar are consistently present. This rock has been graphed as a silty limestone (see Mule coregraph) because most of the material is indeed composed of calcite and technically belongs to the uppermost beds of the Desert Creek cycle. Plane polarized light (40x).

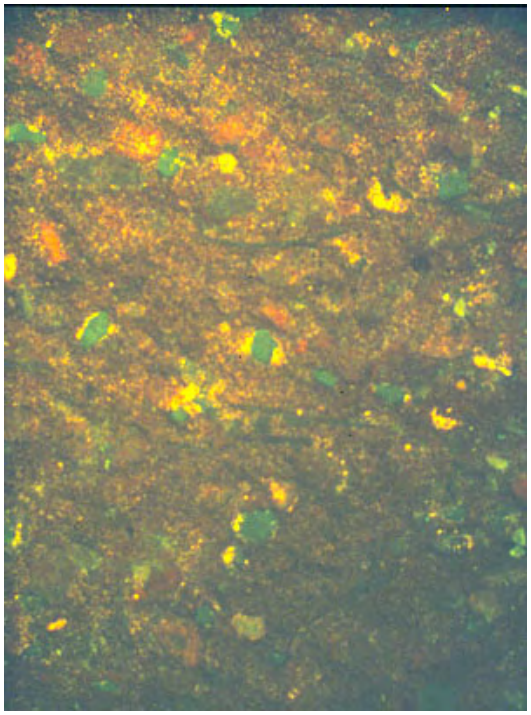

Depth: 5924.2 feet. Higher magnification, reflected light view illustrates the comparative abundance of porosity (orange and light yellow green) in this rock immediately stratigraphically adjacent to the Gothic shale above. Gas production from this limestone is very possible given the effects of hydraulic fracturing. Epifluorescent light with blue-violet filter (100x)

Mule 31-K – 6009.6 ft

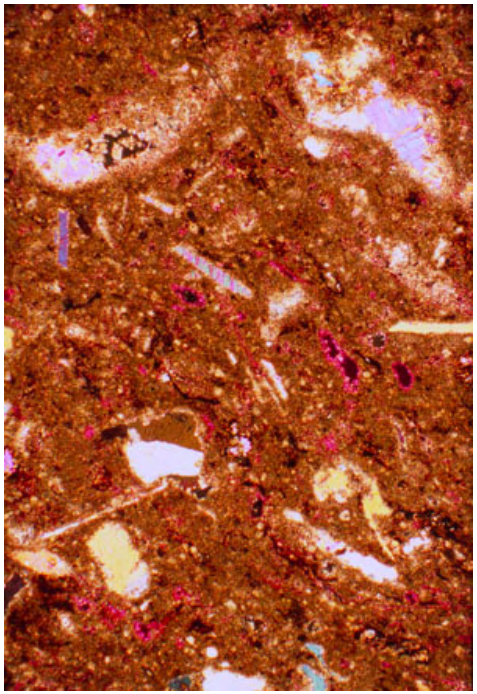

Depth: 6009.6 feet. This limestone is again not represented on any coregraph, but occurs between the Gothic and Chimney Rock shales. This limestone is marked by numerous dissolution features, some of which have been occluded by anhydrite (blue birefringence), located just below the dissolution void in the upper left corner (lath-like grains). Magenta epoxy representing porosity can be seen in spite of the cross-polarization view. Cross-polarized light (40x).

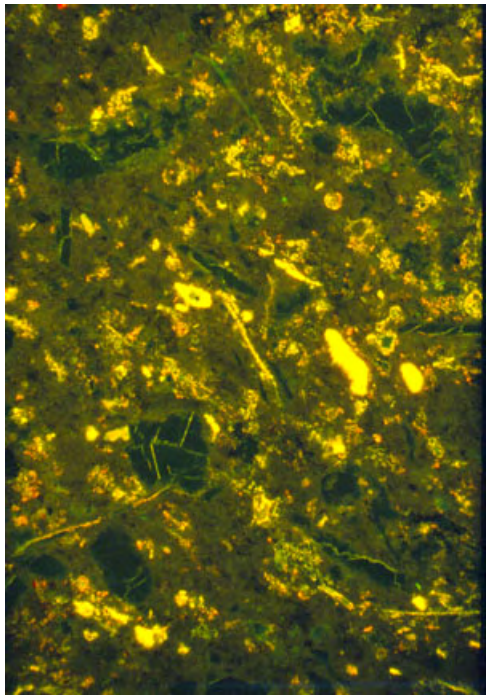

Depth: 6009.6 feet. Reflected light view of the previous reveals both mesopores (light yellow-green) and micropores (orange) present. The latter voids are likely related to microintercrystalline porosity between very small microspar crystals. Whether this limestone is accessed by any shale stimulation treatment is clearly conjecture in this instance because of the "distance" away from either the Gothic stratigraphically above or the Chimney Rock below. Epifluorescent light with blue violet filter (40x).

Mule 31-K – 6099.6 ft

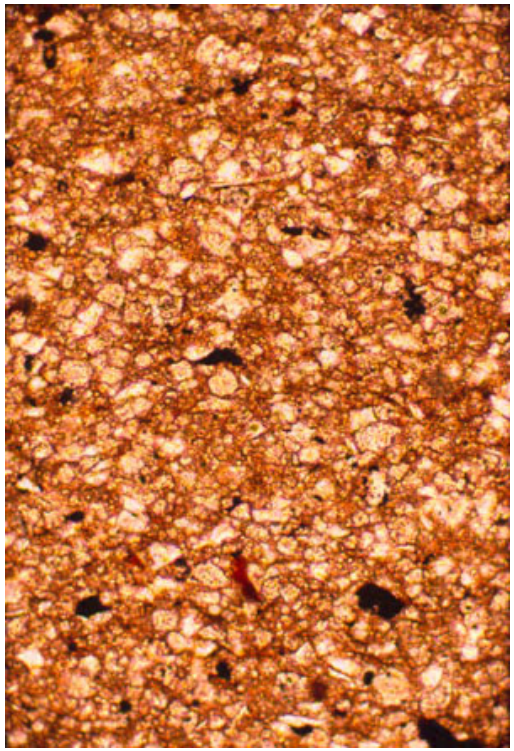

Depth: 6099.6 feet. This carbonate rock is a dolomite that sits almost directly above the Chimney Rock Shale. The dolomite appears almost bimodal because some of the crystals have replaced original quartz or feldspar grains. Some vestiges of white reflect what is left of these original terrigenous clastics. Plane-polarized light (100x).

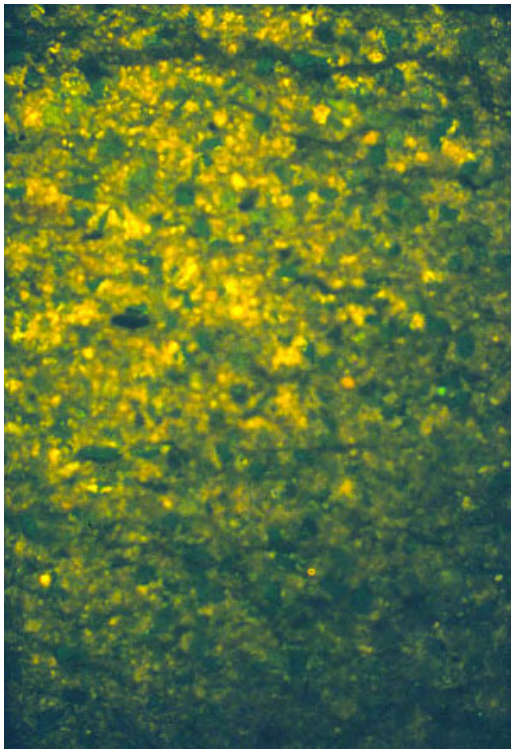

Depth: 6099.6 feet. The refrain is the same for much of the shale-associated strata, as clear micropores are seen in the form of orange hues. Not only do the thin sections reveal this microporosity, but the reader should also consult the SEM photomicrographs for even a clearer picture. Epifluorescent light with blue-violet filter (100x).

Mule 31-K – 6102.4 ft

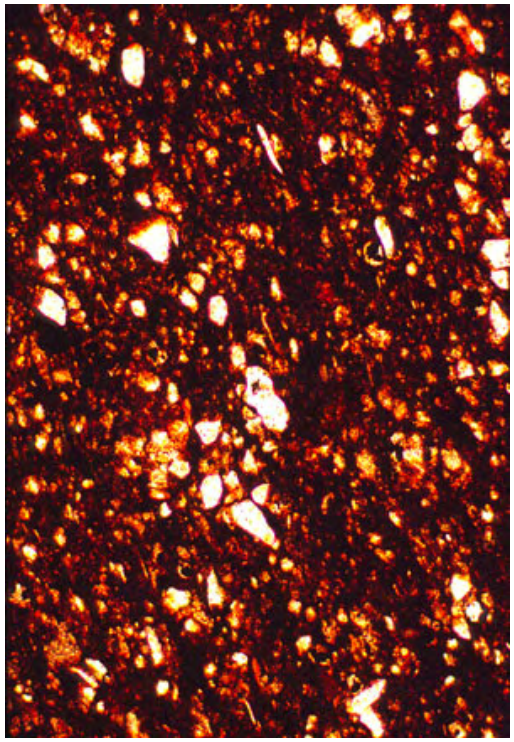

Depth: 6102.4 feet. Upper example of an organic Chimney Rock mudstone where terrigenous clastics are clearly entombed in the chloritic, illitic, and slightly smectitic matrix mud. Plane-polarized light (100x).

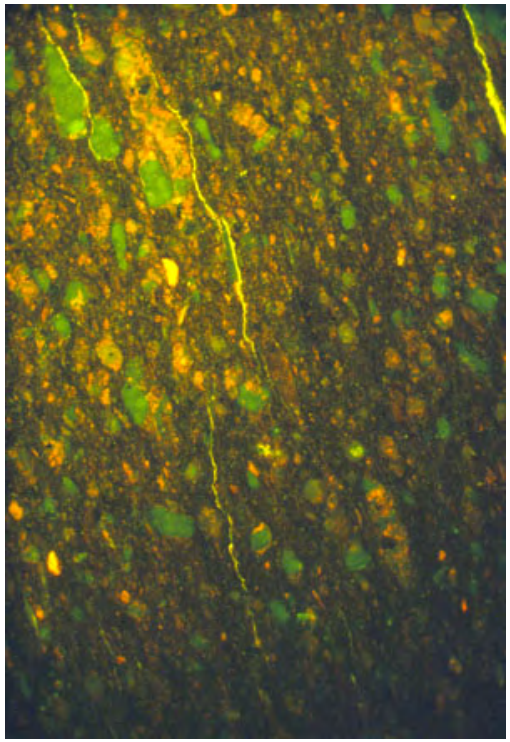

Depth: 6102.4 feet. Terrigenous material appears green in this reflected light view, however, clay microporosity is again indicated in by the orange portions of the photomicrograph. Microfractures are likely artifacts of coring or of thin section preparation, and are probably not natural cracks. Epifluorescent light with blue-violet filter (100x).

Mule 31-K – 6106.95 ft

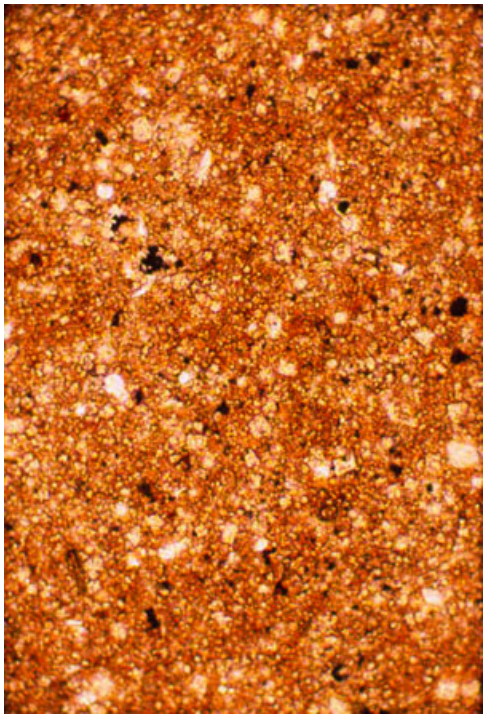

Depth: 6106.95 feet. A view of a silty dolomite bed situated between Chimney Rock shale sequences. These dolomite interbeds are reasonably common in core, and possess a low gamma ray signature on openhole logs. Because these interbeds are again microporous, petrophysical recognition of such interbeds is important for understanding the influence of lithologies, other than mudstones, on potential production results. Plane-polarized light (100x).

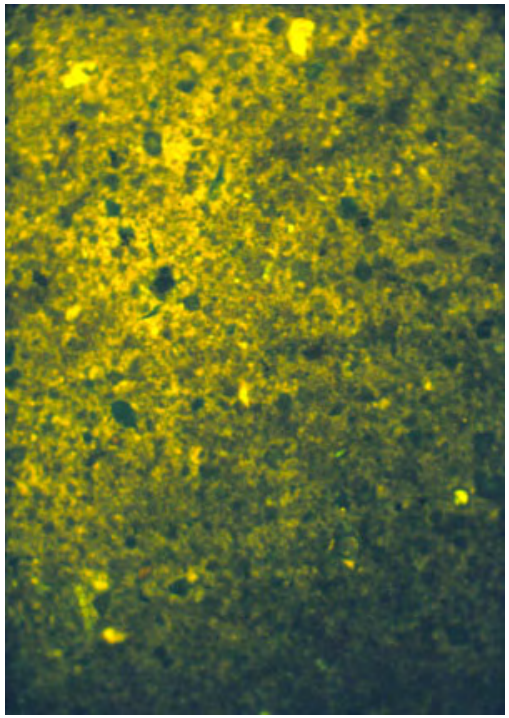

Depth: 6106.95 feet. Epifluorescent view of the previous reveals both mineral (yellow green) and microintercrystalline porosity (orange) fluorescence. Although this photo is slightly out of focus, the green and black shades represent the opaque grains reflective of quartz and/or dolomite compositions. In addition to the matrix microporosity seen here, this interval is beset by an abundance of subvertical natural fractures, both filled and partially filled, best seen in slabbed core. Epifluorescent light with blue-violet filter (100x).

Mule 31-K – 6113.45 ft

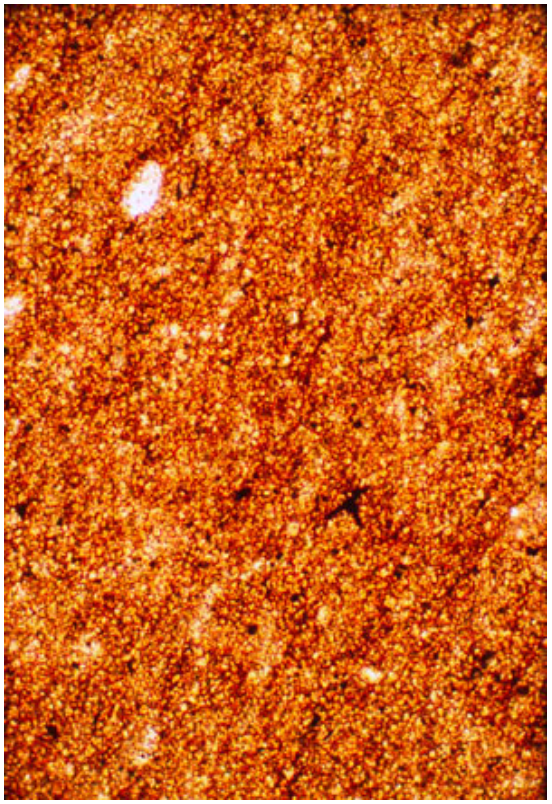

Depth: 6113.45 feet. This dolomite interbed is more solidly dolomitic with less obvious terrigenous material. Nonetheless, this unit again occurs stratigraphically between Chimney Rock mudstone intervals. While this unit looks tight, one could argue that any sort of porosity/permeability combination might be encountered in these associated dolomitic examples. Plane-polarized light (100x).

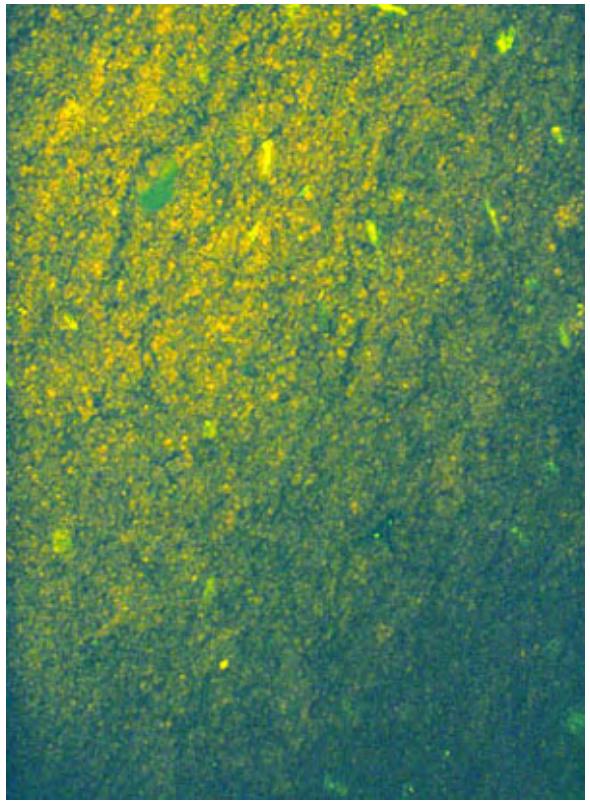

Depth: 6113.45 feet. Orange microporous shades are still recognized in the reflected view of the previous photomicrograph. Details of such porosity are best seen in the scanning electron microscopy studies, also appended to the written report. Epifluorescent light with blue-violet filter (100x).

Appendix C –
Scanning Electron Microscopy

SEM PLATE 1
Mule 31-K well, Chimney Rock, Depth 6099 ft

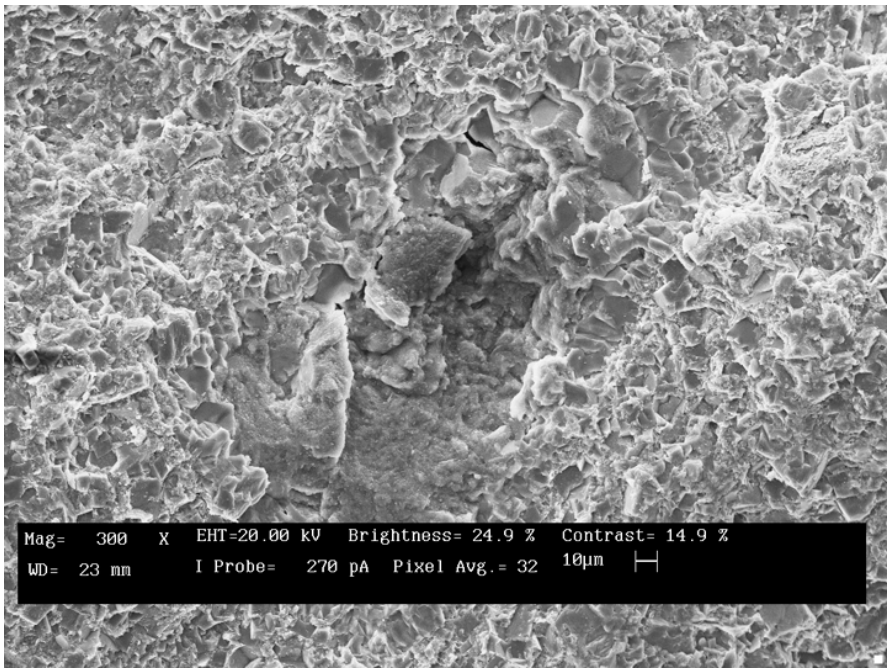

General texture overview of a dolostone characterized by euhedral crystals of dolomite that are about 10 microns wide and sparse silt. A calcareous microfossil is shown in the middle of the image. (Scale bar = 10 microns)

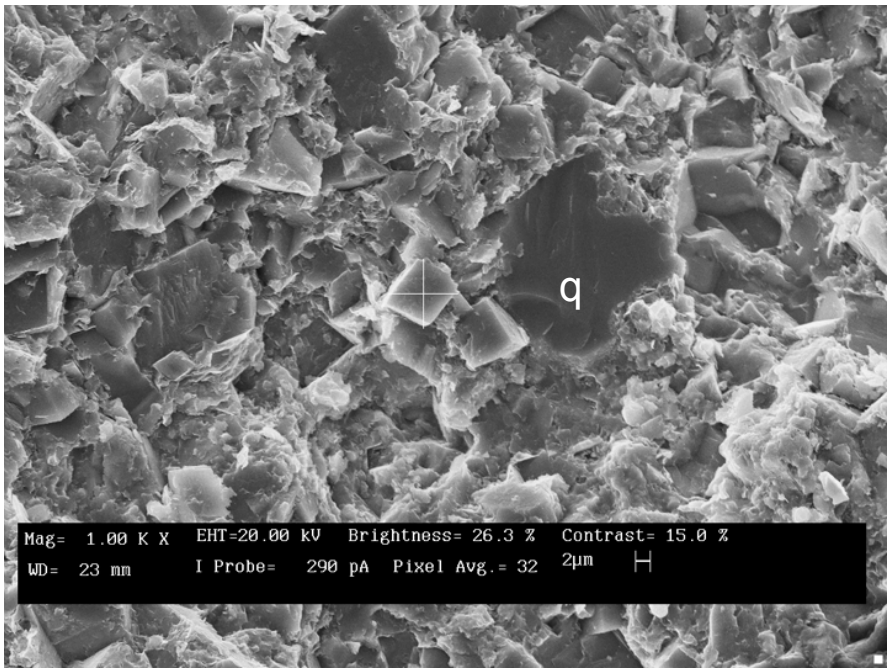

Visible porosity in the dolostone is significantly reduced by authigenic cements including clays that fill most intercrystalline micropores between euhedral dolomite (+) and coat detrital quartz silt (q). (Scale bar = 2 microns)

SEM PLATE 2
Mule 31-K well, Chimney Rock, Depth 6099 ft

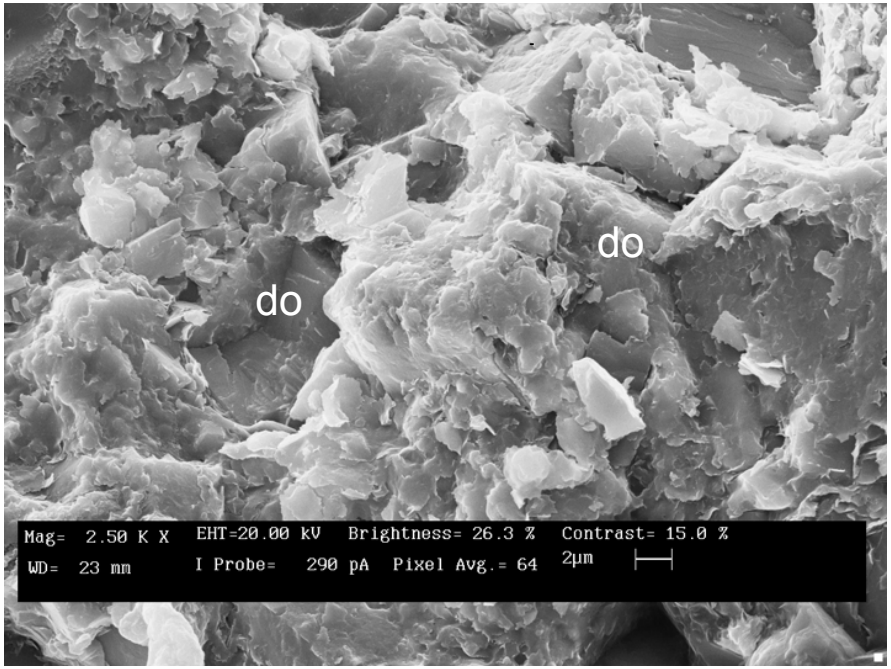

Closer view highlighting siliceous cement occluding interstitial cavities between dolomite crystals (do). Microporosity is minimal here, and pores are less than 1 micron wide. (Scale bar = 2 microns)

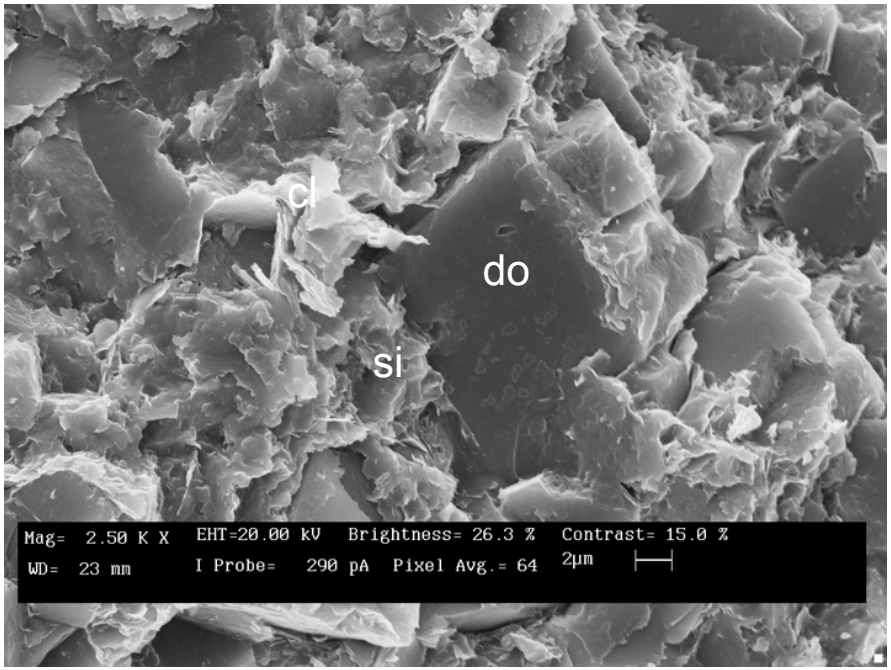

Another closer view at same magnification showing authigenic cements such as silica (si) and flaky minerals including chlorite (ch) filling intercrystalline cavities between dolomite rhombs (do). (Scale bar = 2 microns).

SEM PLATE 3
Mule 31-K well, Chimney Rock, Depth
6102.4 ft

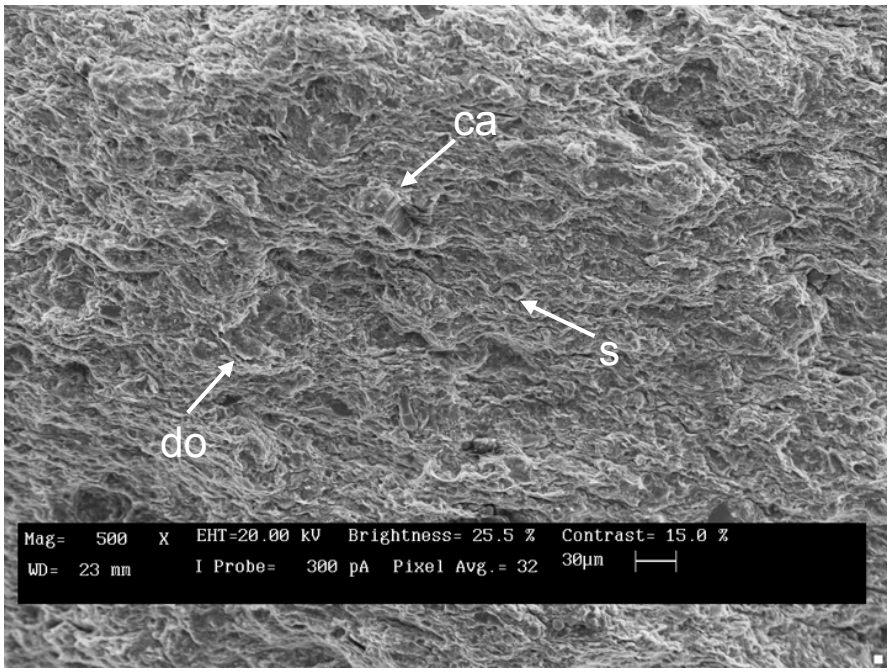

Overview of dolomitic/calcareous mudstone that is characterized by a wavy-laminated matrix primarily composed of clay minerals. Silt-size crystals and concretions of calcite (ca) and dolomite (do) are dispersed in the matrix together with detrital silt (s). (Scale bar = 30 microns)

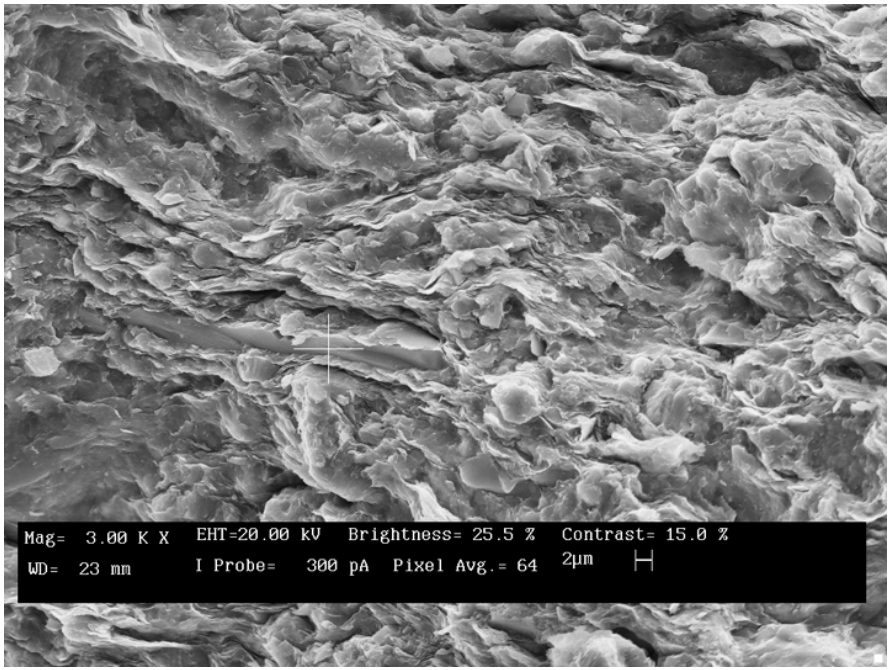

Closer examination reveals considerable amounts of calcareous and dolomitic cements admixed with laminated clay minerals. These cements reduce primary porosity that mainly includes flattened intercrystalline micropores between clay minerals. (+ = calcite shell fragment) (Scale bar = 2 microns)

SEM PLATE 4
Mule 31-K well, Chimney Rock, Depth 6102.4 ft

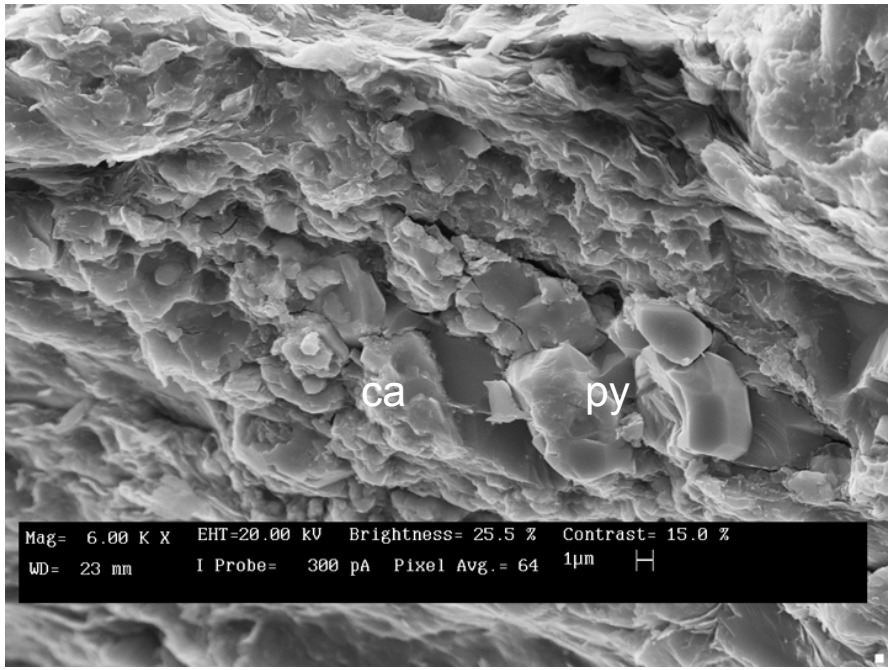

Detailed view showing authigenic cements such as pyrite (py), calcite (ca), and dolomite occluding intercrystalline cavities between layers of clay minerals. (Scale bar = 1 micron)

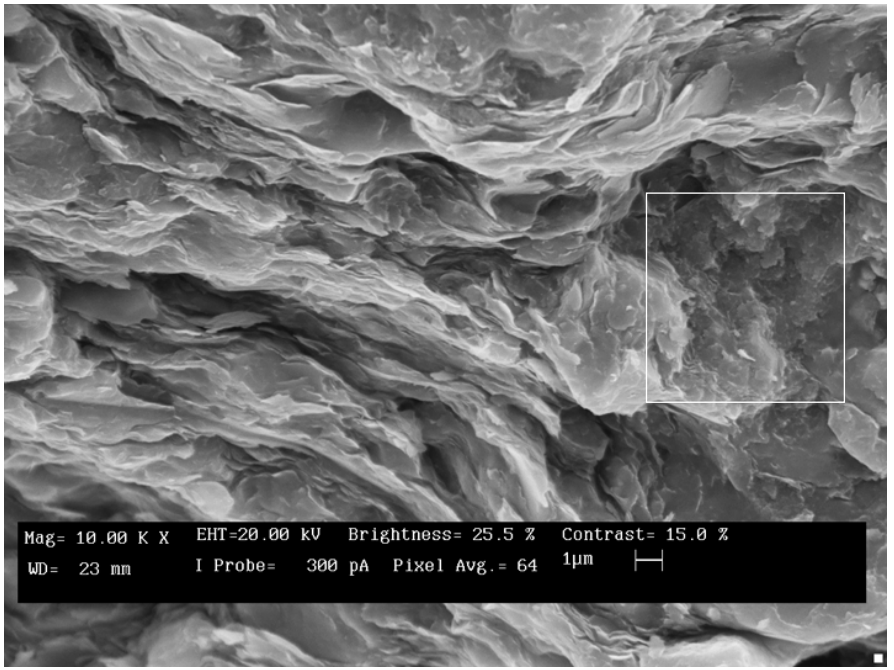

More detailed view of flattened intercrystalline micropores (0.5-1 micron wide) between layers of clay mineral. Stippled texture shown on the right (box) indicates possible amorphous kerogen. (Scale bar = 1 micron)

SEM PLATE 5
Jefferson State 4-1, Sample G, 6051 ft,
Gothic Shale

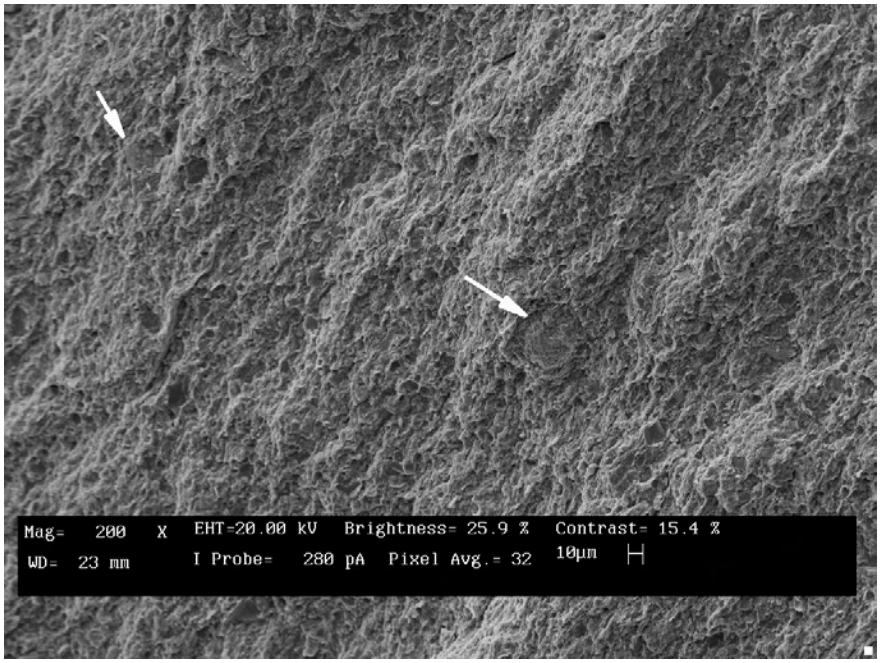

Poorly laminated mudstone at low magnification. Whole view EDX produces peaks for Si, O, Ca, Al, Mg, K and Fe in descending order. Likely minerals include clays (illite and possibly chlorite), dolomite, and quartz. Several pyrite framboids (arrows) are visible in this image. (Scale bar = 10 microns)

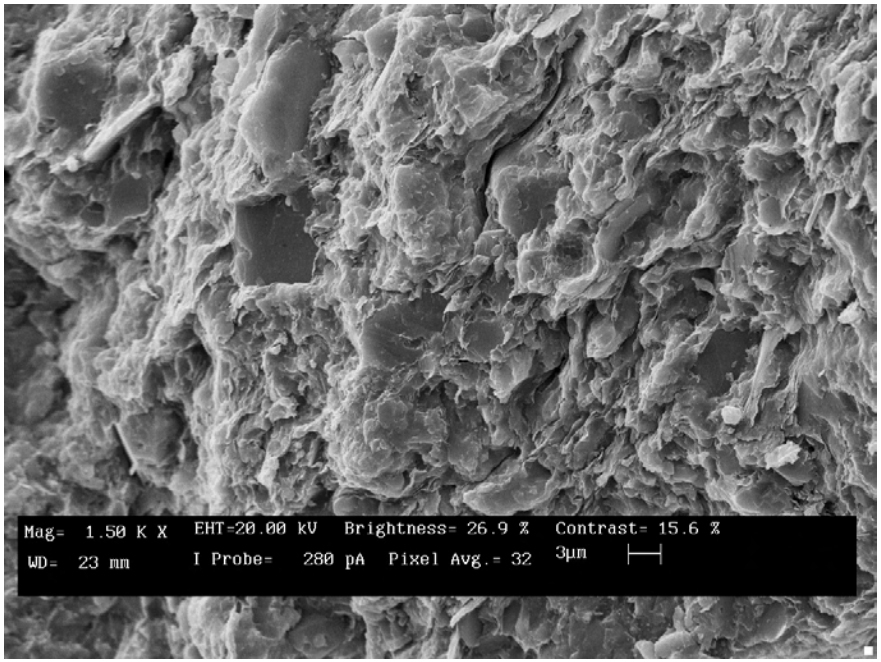

At higher magnification, silt-sized calcite and non-ferroan dolomite grain replacements populate a matrix of wavy and crenulated clay flakes. Secondary minerals are identified by spot EDX analysis. The most common pores are intercrystalline micropores between clay flakes. (Scale bar = 3 microns)

SEM PLATE 6
Jefferson State 4-1, Sample G, 6051 ft,
Gothic Shale

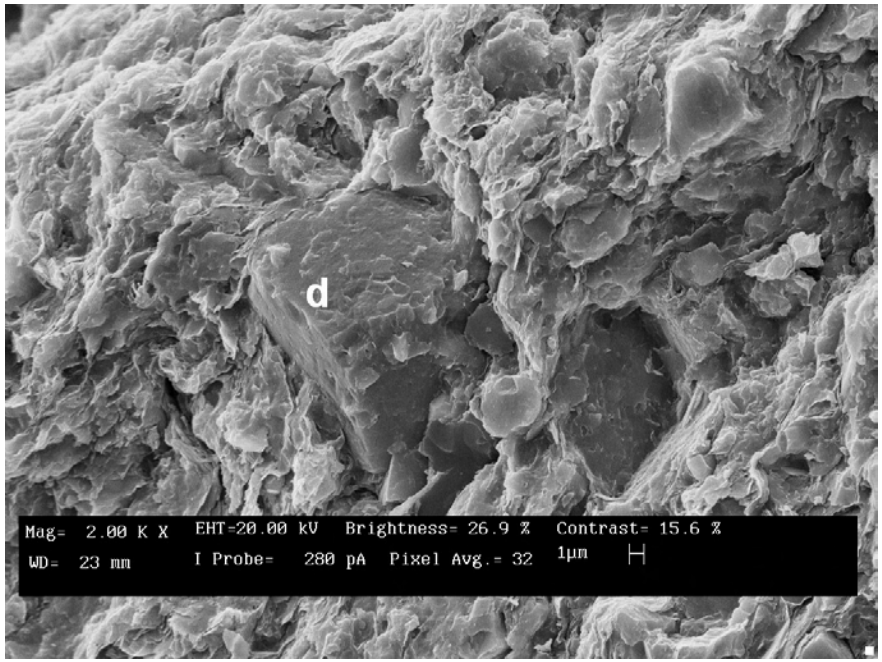

Rectangular dolomite crystal embedded in clay matrix. Spot EDX for the crystal (d) shows an elemental composition of Ca, Mg and O. Clay composition can not be ascertained without XRD, although individual particles show EDX spectra corresponding to illite (Si, O, Al, and K) and probable chlorite (Si, O, Al, Mg and Fe). (Scale bar = 1 micron)

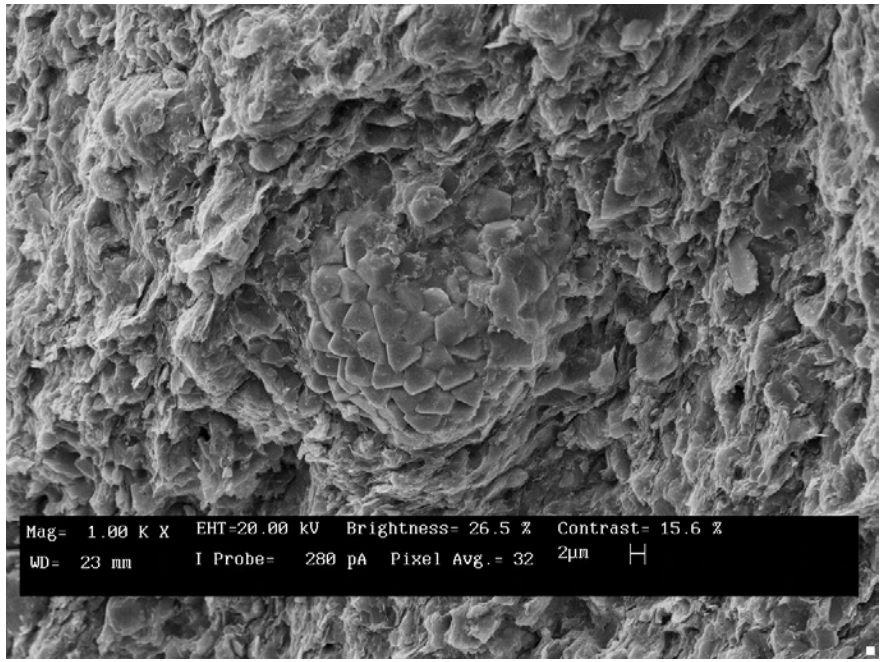

Pyrite framboid in shale at medium magnification. Pyrite appears to be relatively common in the sample. Large peaks for sulfur and iron dominate the spot EDX spectrum, confirming the pyrite composition. Ragged and weakly aligned flakes make up the matrix, which is likely a mixture of detrital clays. (Scale bar = 3 microns)

SEM PLATE 7
Jefferson State 4-1, Sample H, 6070 ft,
Gothic Shale

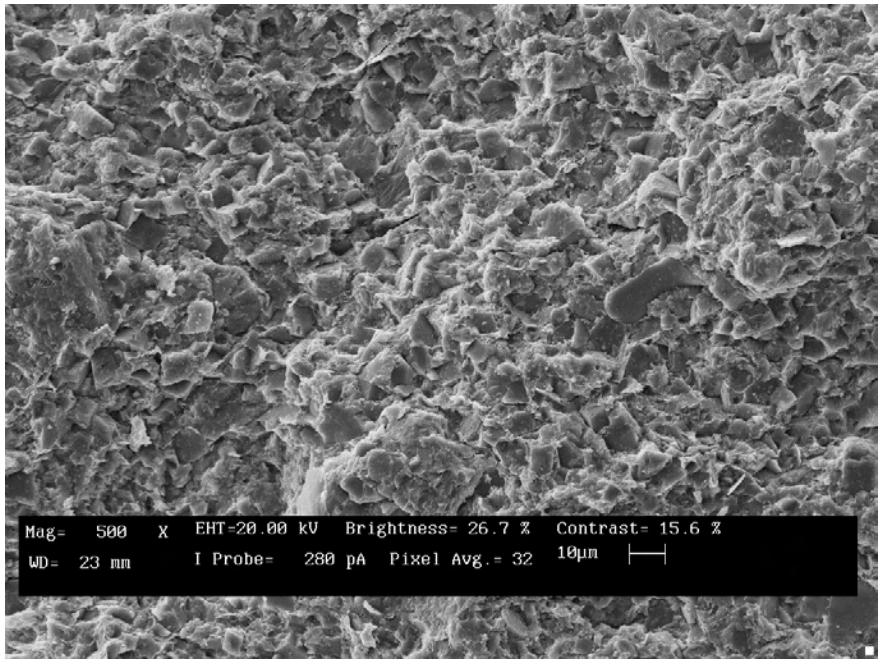

Overview of mudstone texture dominated by interlocking, subhedral dolomite crystals. Porosity is likely minimal in this sample. Whole view EDX for the area shown here is presented in the next image.

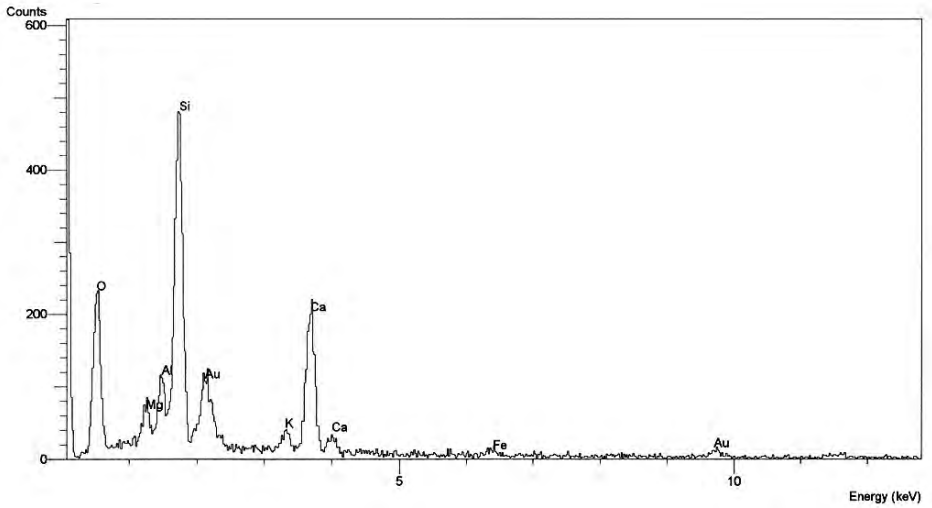

Whole view EDX spectrum corresponding to the area in the previous image. Peaks for Si, O, Al and K likely indicate illite, whereas Ca, Mg and O peaks denote dolomite. A likely interpretation is a diagenetic dolomite overprint on an illitic mudstone matrix. The small iron peaks are more likely associated with clays than dolomite: EDX on individual dolomite crystals show no Fe component.

SEM PLATE 8
Jefferson State 4-1, Sample H, 6070 ft,
Gothic Shale

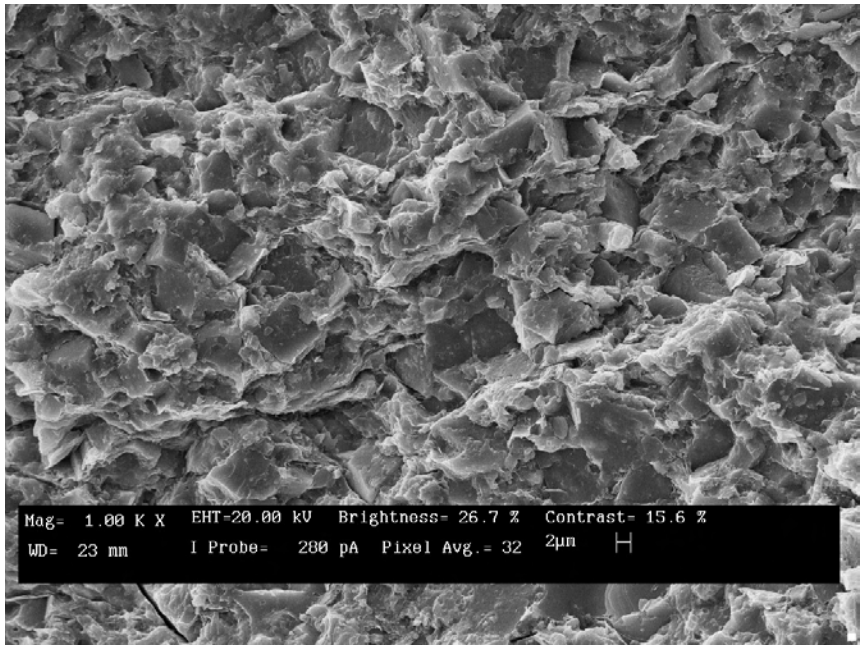

Higher magnification view of dolomitic mudstone highlighting packets of clays (preferred alignment lower left to upper right) sandwiched between dolomite crystals. The tightly crystalline fabric leaves little visible microporosity. (Scale bar = 2 microns)

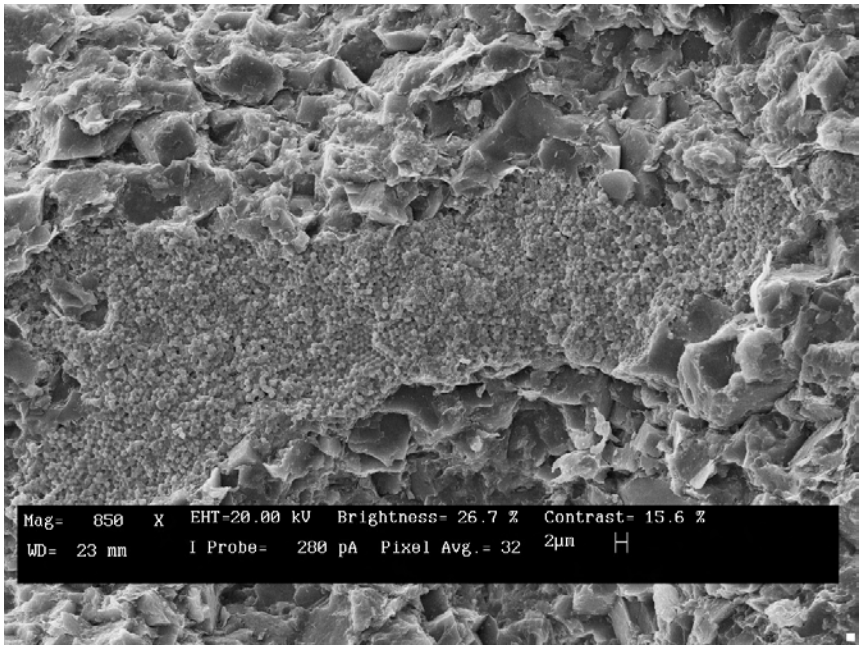

Another view of dolomitic mudstone showing pyrite replacing a globular form, most likely organic in origin. Pyrite is relatively rare in the rest of this SEM sample. (Scale bar = 2 microns)

SEM PLATE 9
Jefferson State 4-1, Sample H, 6070 ft,
Gothic Shale

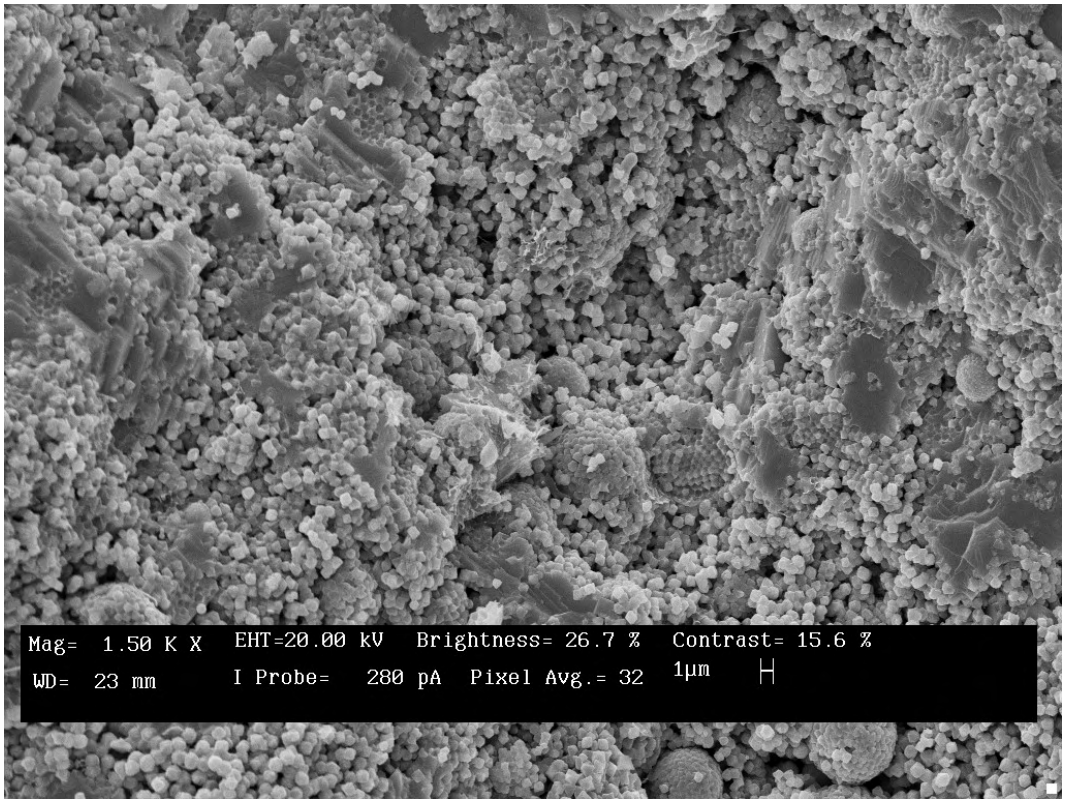

Internal structure of the pyrite nodule shown in the previous image. The fabric consists of a collection of pyrite framboids as well as loose microcrystals. Nanometer-scale pores are visible in this image. (Scale bar = 1 micron)

SEM PLATE 10
Jefferson State 4-1, Sample L, 6192.5'
Chimney Rock Shale

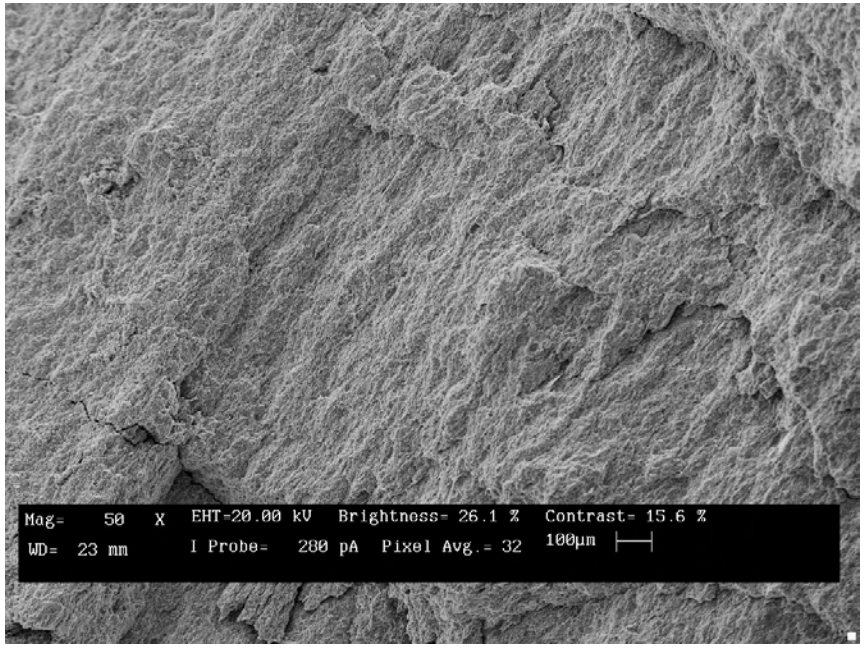

SEM image of shale at very low magnification exhibiting a blocky, crumbly and soft texture with moderate lamination. Little or no silt or sand-sized material is observed, identifying the sample as shale rather than mudstone. (Scale bar = 100 microns)

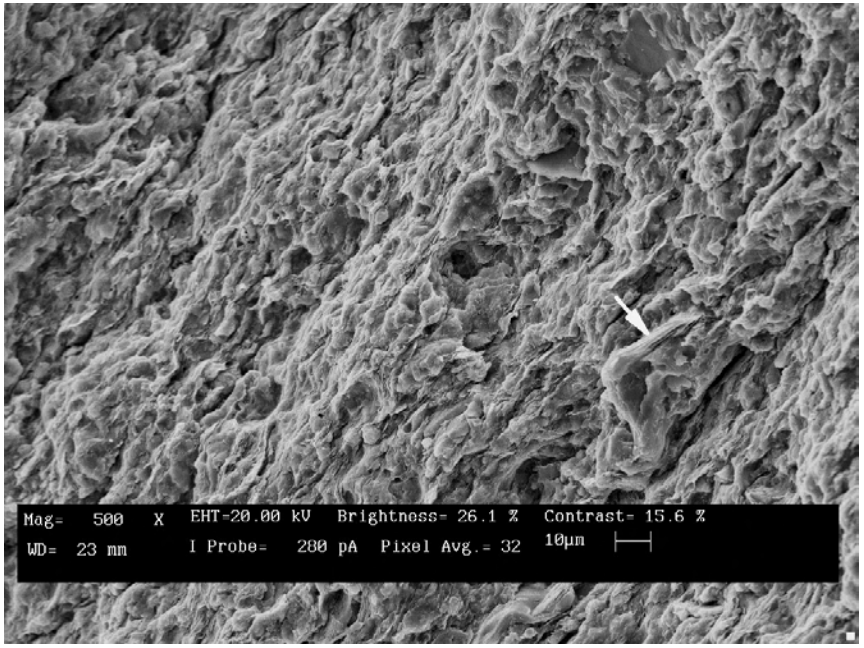

Slightly more magnified view highlighting a laminated fabric of crenulated clays. A mixture of detrital clays is most likely; the large flake (arrow) produces the spot EDX spectrum shown in the next image. Induced stress-release porosity is evident as elongate microfractures parallel to bedding. (Scale bar = 10 microns)

SEM PLATE 11
Jefferson State 4-1, Sample L, 6192.5'
Chimney Rock Shale

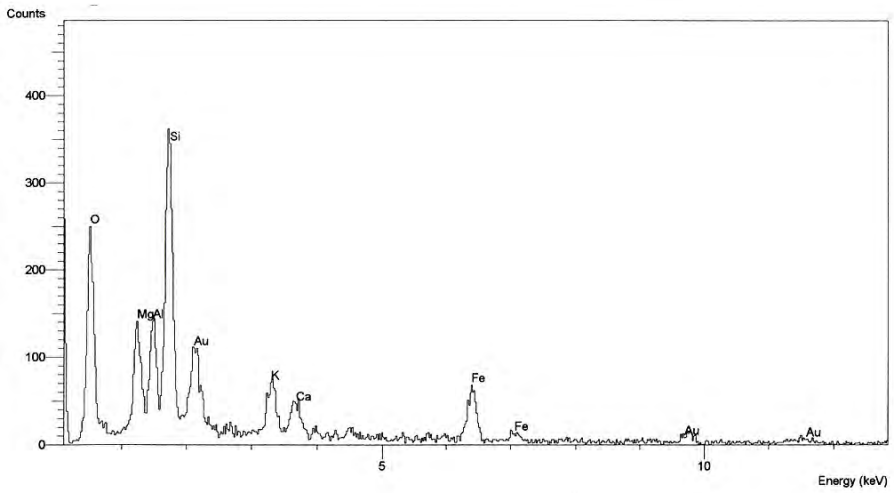

Elemental spectrum for the clay flake in the previous image (arrow). In addition to Si, O, and Al peaks indicative of clay, medium-sized peaks for Mg and Fe suggest a chlorite composition. The K peak likely denotes illite, whereas the Ca peak could indicate intermixed illite/smectite. Gold peaks reflect sample coating.

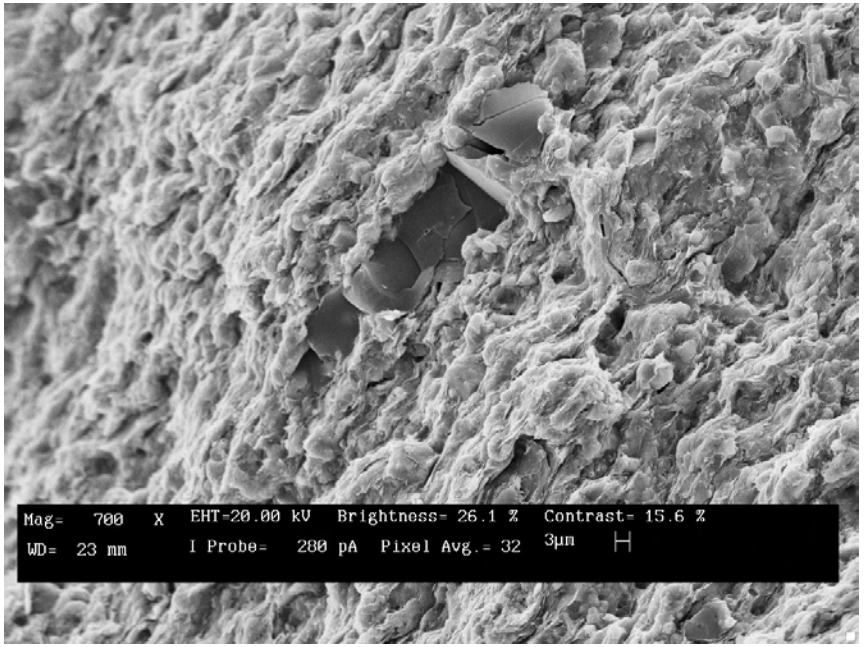

The flattened carbonaceous particle at center produces a poor elemental spectrum in spot EDX analysis, with a small carbon peak. Discrete organic particles are sparsely distributed throughout both Chimney Rock samples (L and M). EDX identifies the clays as a mixture of illite and chlorite. (Scale bar = 3 microns)

SEM PLATE 12
Jefferson State 4-1, Sample L, 6192.5'
Chimney Rock Shale

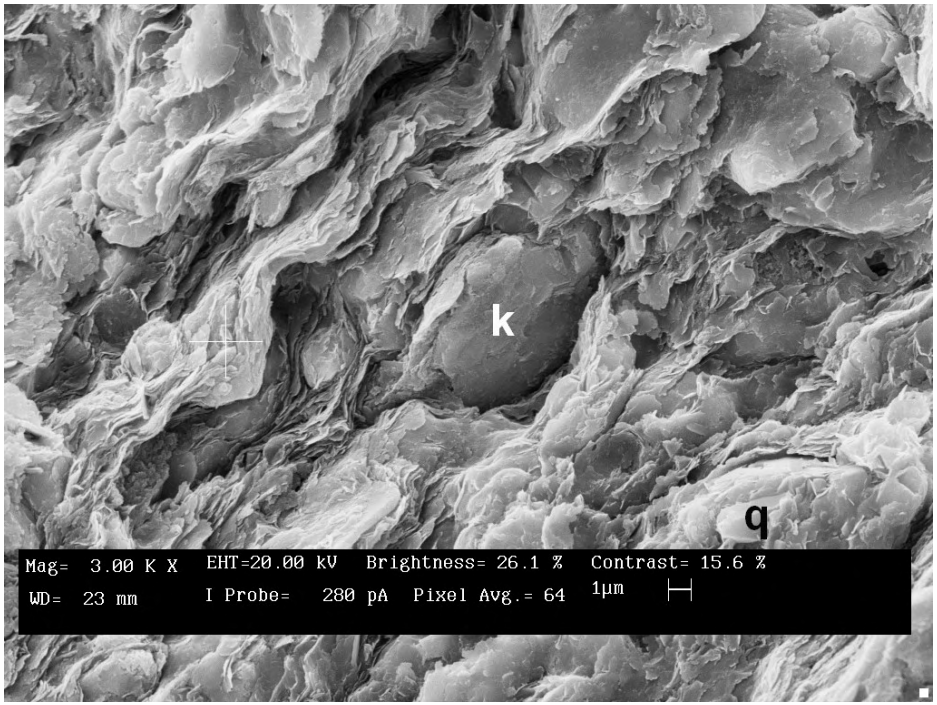

Quartz (q) and feldspar (k) silt grains prop open voids between clay flakes in this high magnification view. Micropores average 1-2 microns in size. The crenulated clay flake at left (+) produces a spectrum dominated by Si, O, Ca, Al, Mg and K peaks. Elemental composition combined with morphology, although not definitive, suggests a mixed illite, illite/smectite, and chlorite composition. (Scale bar = 1 micron)

SEM PLATE 13
Jefferson State 4-1, Sample M, 6195.5'
Chimney Rock Shale

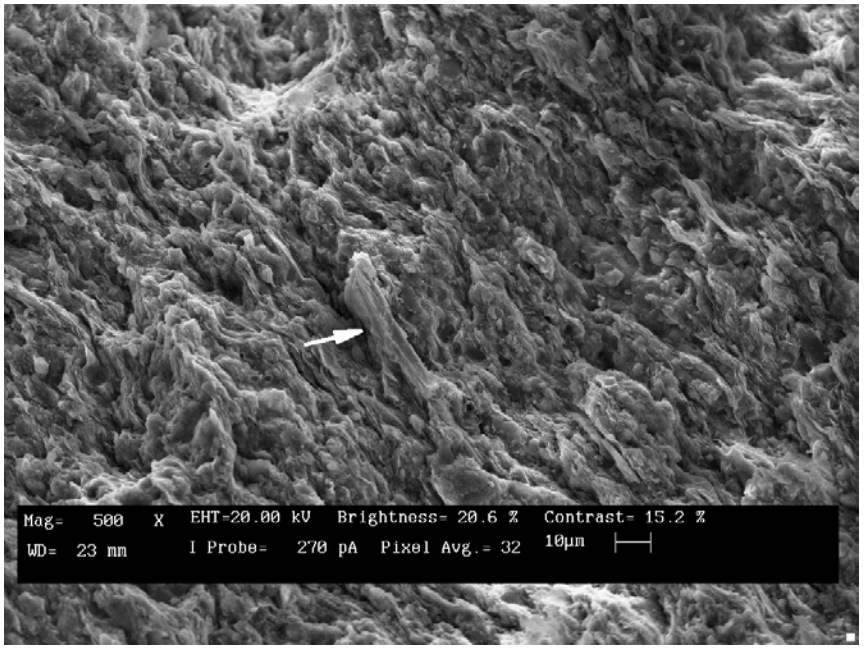

Overview of shale texture exhibiting weakly developed laminae composed of stacked and crenulated clay flakes. Whole view EDX analysis of the area in the image shows major peaks for Si, Al, and O, peaks of lesser magnitude for Mg and K, as well as smaller Ca and Fe peaks. A matrix composition of mixed illite, illite/smectite, and chlorite is probable. Chlorite does not seem to be particularly iron-rich (Mg > Fe peaks in EDX). The flake at center (arrow) is most likely a degraded mica (Si, Al, O, K > Fe and Ca). (Scale bar = 10 microns)

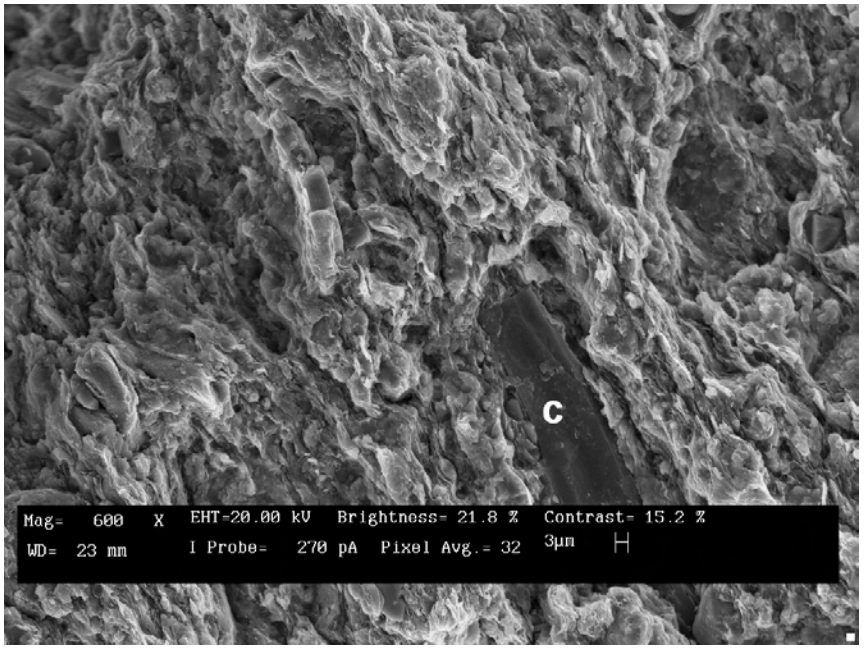

Carbonaceous particles (c) aligned parallel to bedding in shale. Crenulated shapes of clay flakes, irregularities introduced by diagenetic cement crystals, and admixed organic particles all create open micropores in the heterogeneous shale matrix. (Scale bar = 3 microns)

SEM PLATE 14
Jefferson State 4-1, Sample M, 6195.5'
Chimney Rock Shale

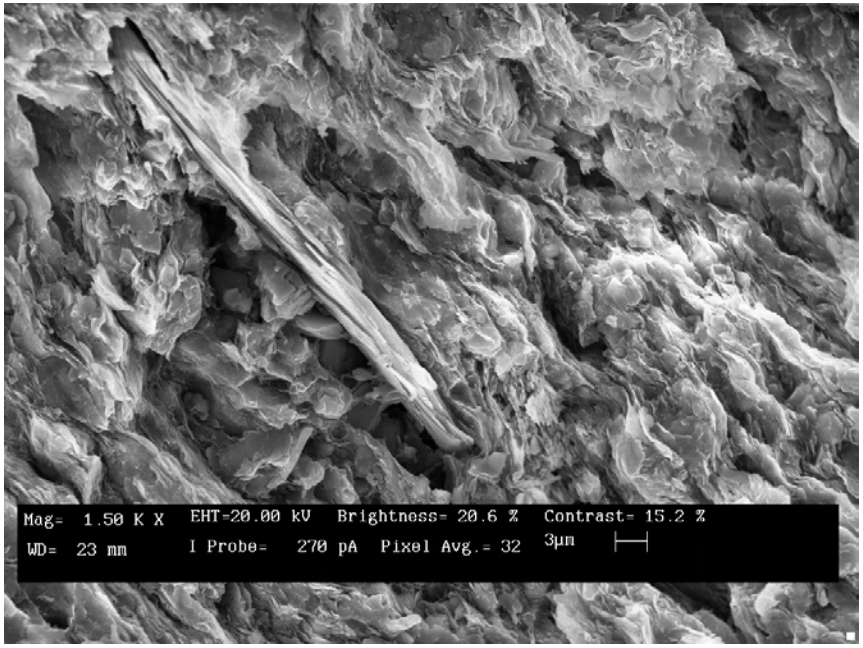

The long, straight mica grain at left is interpreted as biotite; EDX produces a spectrum with prominent Si, O, Al = Fe > Mg > K, Ca). The surrounding matrix hosts dense clusters of wavy illite and possibly magnesium-rich chlorite or illite/smectite. Elongate intercrystalline micropores are evident, typically measuring 0.5-2 microns in size. (Scale bar = 3 microns)

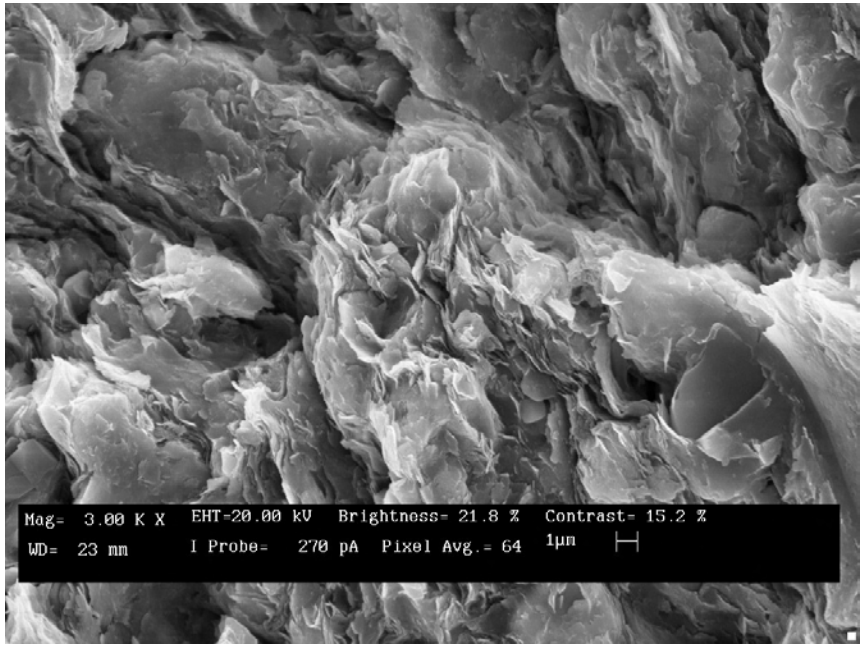

Higher magnification of whorled habit in clay flakes. Natural intercrystalline micropores (< 1 micron) as well as more linear, stress-release or dehydration fractures are visible in this image. Spot EDX analysis for the clay cluster at center reveals peaks for Si, Al, O, Mg and K, in order of magnitude. A mixed composition of illite and either magnesium smectite or chlorite is inferred. (Scale bar = 1 micron)

Appendix D - Fracture Analysis
Jefferson State 4-1

Depth (ft)	Morphology	Comments
5860.1	filled-oblique	
5900-5902	filled-horizontal, filled-subhorizontal	multiple fracture
5904.4	filled-oblique	two main fractures
5904.8	filled-oblique	calcite filled
5909.2	partially filled-oblique	
5914	partially filled-subhorizontal	
5916-5917	partially filled-horizontal, partially filled-subhorizontal	multiple fracture
5918.2-5918.8	partially filled-vertical to horizontal, open-vertical	small vertical fractures connecting layered horizontal fractures
5922.3	open-vertical	
5923.7-5925.2	partially filled-vertical	very thin calcite cement
5930.2	open-vertical	
5930.3	open-vertical	two main fractures
5931.4	partially filled-vertical	two main fractures
5939.4	filled-horizontal	dish shaped
5941.1-5943.8	filled-vertical to partially filled-vertical	calcite cement, possibly 2 fractures?
5943.9	filled-vertical	three fractures
5944.1	partially filled-vertical, open-vertical	
5944.5	partially filled-vertical	3” visible length
5945-5945.3	partially filled-vertical	calcite cement, two main fractures
6003.6		base of anhydrites (no frac)
6005.1	filled-vertical	
6006-6006.4	partially filled-vertical	
6006.8	open-vertical	two main fractures
6007.1-6007.5	open-subvertical	
6007.8-6008	open-vertical	
6008-6009	filled-vertical, partially filled-vertical, open-vertical	12 small fracture planes
6009-6009.6	open-vertical, partially filled-vertical	6 small fractures
6010-6022.5		pervasive microfractures
6013-1-6014	filled-vertical, partially filled-vertical, open-vertical	numerous fracture planes
6013.8-6014.1	filled-vertical	
6014.1-6015.5+	open-vertical	
6031-6033.6	filled-vertical	
6034.3-6036.35	filled-vertical	
6034.3-6039.5		
6036.6-6041.3	partially filled-vertical, open-vertical	more cementation toward top of fracture
6036.7-6039	filled-vertical,partially filled-vertical	
6039.6-6041.3	filled-vertical	two main fractures

Appendix E - XRD Mule 31-K

Sample ID	**2**	**3**
Depth (Ft)	**6102.40**	**6106.95**
Quartz	25	30
K-Feldspar	3	0
Plagioclase	4	0
Calcite	12	1
Siderite	0	0
Ankerite/Fe-Dolomite	2	6
Dolomite	9	41
Pyrite	5	1
Fluorapatite	1	1
Magnetite	0	1
Total Non-Clay	**60%**	**81%**
Smectite	0	5
Illite/Smectite (I/S)	19	0
Illite+Mica	19	9
Kaolinite	0	0
Chlorite	2	5
Total Clay	**39%**	**19%**
Grand Total	**100**	**100**
Relative Clay Abundance In Bulk Sample		
% I/S Expandability	*25*	*25*
Smectite	0	25
Illite/Smectite (I/S)	48	0
Illite+Mica	47	47
Kaolinite	0	0
Chlorite	5	28
Total	**100**	**100**
Total Expandable Clay	**5**	**5**

(These are Chimney Rock samples)